Comparison of Prediction Models for Sonic Boom Ground Signatures Under Realistic Flight Conditions

aerospace

MDPI

Article

Comparison of Prediction Models for Sonic Boom Ground Signatures Under Realistic Flight Conditions

Jacob Jäschke [1,*], Samuele Graziani [2], Francesco Petrosino [3], Antimo Glorioso [4] and Volker Gollnick [1]

[1] Institute of Air Transportation Systems, Hamburg University of Technology, 21073 Hamburg, Germany; volker.gollnick@tuhh.de
[2] Mechanical and Aerospace Engineering Department, Politecnico di Torino, 10129 Torino, Italy; samuele.graziani@polito.it
[3] Italian Aerospace Research Center (CIRA), 81043 Capua, Italy; f.petrosino@cira.it
[4] Engineering Department, Università degli Studi della Campania "Luigi Vanvitelli", 81031 Aversa, Italy; antimo.glorioso@unicampania.it
* Correspondence: jacob.jaeschke@tuhh.de

Abstract: This paper presents a comparative analysis of simplified and high-fidelity sonic boom prediction methods to assess their applicability in the conceptual design of supersonic aircraft. The high-fidelity approach combines Computational Fluid Dynamics (CFD) for near-field shock analysis with ray-tracing and the Augmented Burgers Equation for far-field propagation through a non-uniform atmosphere, whereas the simplified Carlson method uses analytical approximations for rapid predictions. The comparison across selected climb, cruise, and descent conditions for a supersonic reference aircraft shows that the Carlson method captures general trends in sonic boom behavior, such as changes in peak overpressure and signal duration with varying Mach number and altitude. However, significant deviations are noted under realistic atmospheric conditions, highlighting limitations in the simplified model's accuracy. Common psycho-acoustic metrics were evaluated to assess the potential annoyance on the ground. The results demonstrate that while the simplified method is effective for early-stage design assessments, the high-fidelity model is essential for precise sonic boom characterization under realistic conditions, particularly for regulatory and community impact evaluations.

Keywords: aeroacoustics; semi-empirical methods; sonic boom; shock wave propagation; supersonic

Citation: Jäschke, J.; Graziani, S.; Petrosino, F.; Glorioso, A.; Gollnick, V. Comparison of Prediction Models for Sonic Boom Ground Signatures Under Realistic Flight Conditions. *Aerospace* **2024**, *11*, 962. https://doi.org/10.3390/aerospace11120962

Academic Editor: Bosko Rasuo

Received: 18 October 2024
Revised: 15 November 2024
Accepted: 17 November 2024
Published: 22 November 2024

1. Introduction

A sonic boom is a phenomenon that occurs when an object travels through the air faster than the local speed of sound, creating shock waves that propagate to the ground. These shock waves result in a loud and sometimes disruptive noise, experienced as a "boom" or "bang" by observers. In aviation, sonic booms have been associated with supersonic flight, which became a significant topic of interest during the development of supersonic aircraft like the Concorde and various military jets during the second half of the last century [1].

The importance of understanding sonic booms is driven by both their environmental impact and the regulatory challenges they pose. When aircraft fly at supersonic speeds, the sonic boom causes noise pollution, which has historically led to restrictions on supersonic flight over land in many countries, including the United States and European countries [2]. This limitation has been a major hurdle for the development of commercial supersonic travel [3].

With renewed interest in civil supersonic travel, especially with emerging aircraft concepts [4–6], it has become crucial to accurately predict and mitigate the effects of sonic booms on the community on the ground. Advances in computational methods and atmospheric modeling have improved the ability to predict ground-level sonic boom signatures under various flight conditions [7]. A clear comprehension of these predictions

is crucial for the engineering of quieter supersonic aircraft, which could facilitate a broader acceptance of supersonic travel or enable supersonic overland flight. From the standpoint of regulatory authorities, these predictions also provide insights for the development of future noise regulations pertaining to sonic booms.

Over the last decades, the National Aeronautics and Space Administration (NASA) has put remarkable effort into the development of a low-boom aircraft demonstrator which aims to minimize the nuisance caused by the sonic boom during supersonic flight. The associated test campaign aims to provide reference measurements for the definition of future international standards for sonic booms over land [8]. The definition of future regulations relies on the definition of suitable acoustic metrics, that correlate with the annoyance of sonic boom for the population on the ground, and on defining the acceptable threshold values for the selected metrics [9]. Relevant metrics need to account for the short, impulsive character of the sonic boom and should be robust against atmospheric influences [10–12].

To provide insights to regulators and designers, a method for assessing the sonic boom impact in a multidisciplinary optimization environment during the conceptual design phase of aircraft is sought. In this context, efficient and fast methods to quantify sonic boom effects are crucial. The authors build upon their experience with two methodologies for predicting sonic booms, each offering distinct advantages.

The first method is a high-fidelity approach that involves two stages to model the sonic boom phenomenon as shown in Figure 1. In the first stage, Computational Fluid Dynamics (CFD) simulations are performed to analyze the near-field shock wave behavior, capturing the generation of the shock wave caused by the supersonic velocity of an aircraft [13]. The second stage involves far-field propagation, where ray tracing is employed to simulate the propagation of the shock wave through a non-uniform atmosphere. This process is governed by the Augmented Burgers Equation, a non-linear propagation model that incorporates steepening effects for sound waves, as described by Cleveland [14] and applied by Rallabhandi [15] to sonic boom prediction.

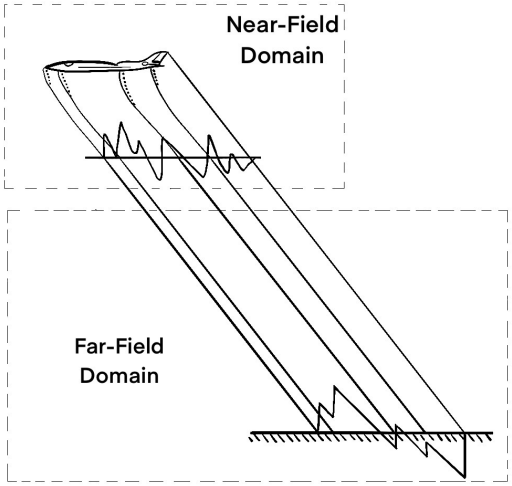

Figure 1. Simulation domains for state-of-the-art sonic boom prediction. The near-field domain is computed via CFD methods while the far-field domain accounts for the atmospheric variations and is modeled with a combination of ray-tracing and a non-linear wave equation. Adapted from [16].

While this approach provides highly accurate predictions, it is computationally intensive, requiring significant processing time for both the CFD simulations (ranging from hours to days) and the non-linear far-field propagation (minutes to hours).

In contrast, the Carlson method [17] offers a simplified and rapid approach to sonic boom assessment, providing results within seconds. This method approximates the key characteristics of the typical sonic boom N-wave by neglecting some of the detailed atmo-

spheric parameters accounted for in the higher-fidelity method. The trade-off between accuracy and computational efficiency motivates a comparison of these two methods under realistic flight and atmospheric conditions. The question is, to what extent can the simplified Carlson method offer sufficient accuracy for use in the early stages of aircraft design when integrated into a design tool, where quick assessments of sonic boom impact are necessary for innovative supersonic configurations?

To effectively integrate analytical methods within a multidisciplinary framework, it is essential to evaluate their validity under realistic flight conditions, extending beyond the cruise phase. Thus, the aim of this paper is to quantify the order of deviation that a simplified analytical sonic boom method like Carlson introduces when assessing a realistic supersonic flight scenario, for which climb and descend flight phases are also considered. Recent studies have shown interest in the evaluation of fast methods for predicting sonic boom at the conceptual design stage [18–22].

Therefore, a Mach 2 supersonic Concorde-like configuration is evaluated under three different flight states along the mission profile, for which the sonic boom impact is computed by both, the higher-fidelity and simplified methods. This comparison aims at giving useful insights for the development of a multi-disciplinary optimization framework for the MORE&LESS project [23]. The project's goal is to establish comprehensive environmental assessments of future supersonic aircraft concepts with a new framework called "ESATTO" (Environmentally Sustainable AircrafT Trajectory and Operations).

As the high-fidelity method is capable of accounting for several parameters of a realistic flight scenario, such as different angles of attack, different atmospheric conditions, and off-design flight states, in general, the results of the various high-fidelity simulations will form a range of sonic boom estimations, which will be used as some kind of ground-truth to assess the simplified method under such circumstances. As a side effect, the study presents an extensive sonic boom characterization with a state-of-the-art methodology of the supersonic vehicle under investigation.

The remainder of the paper is structured as follows: Section 2 presents the two different modeling approaches in greater detail, showcases the reference aircraft for the study and describes the atmospheric variations that will be an input for the high-fidelity model. Section 3 presents the obtained results, which are then discussed in Sections 4 and 5, highlighting the main findings of the work.

2. Materials and Methods

The prediction of the annoyance of sonic boom relies on estimating the shock wave behavior caused by an aircraft at speeds higher than Mach 1. To simulate the shock wave behavior, this paper uses an extensive bi-domain approach on the one hand, which computes an acoustic pressure over time signal on the ground (Section 2.1), and a simplified efficient calculation method on the other hand, which estimates the most relevant features of the shock wave on the ground (Section 2.2). Both approaches allow for an assessment of the acoustic properties of the computed sonic boom on ground by a transformation into acoustic metrics (Section 2.3). To finalize the description of this study's setup, the reference aircraft and its operating conditions (Section 2.4) are introduced before the description of the different atmospheric models (Section 2.5) that were used in this study.

2.1. High-Fidelity Sonic Boom Modeling Approach

The high-fidelity approach is separated into two modeling domains: (1) A near-field domain to account for the three-dimensional fluid effects around the aircraft, which is described in Section 2.1.1, and (2), a far-field domain, to account for the impact of the non-uniform atmosphere, which is described in Section 2.1.2.

2.1.1. CFD Near-Field Simulation

In the last decades, computational fluid dynamics (CFD) has undergone numerous improvements in the correct computation of shock waves [24]. Since 2014, NASA has been hosting the AIAA Sonic Boom Prediction Workshop which aims to establish state-of-the-art numerical prediction methods for sonic boom [16,25–27]. The results of the four different workshops held between 2014 and 2022 have defined the methodology for the correct prediction of supersonic shock wave simulation in the near-field domain.

CFD techniques are widely used to study the supersonic flow around an object, due to the strong non-linearity and 3D interactions that occur in the flow field. In the vicinity of a supersonic aircraft, the versatile aerodynamic effects have a major contribution to the shock wave formation. Refraction effects of a non-uniform and moving atmosphere gain more relevance in the regions further away from the aircraft.

Within this work, the results obtained by Graziani et al. [13] are the input for the far-field domain simulation. The near-field simulations were conducted utilizing both, the commercial software ANSYS Fluent 2022 R1 and the open-source SU2 code [28]. Both of these codes employ an unstructured finite-volume approach to solve the Reynolds Average Navier Stokes (RANS) equations. Gradients are computed with a Green–Gauss method [29]. The simulation was performed without a turbulence model, by solving an inviscid Euler equation with an ideal gas assumption. Previously published works indicate the possibility of using Euler equations to correctly evaluate the shock waves of a supersonic configuration [30–33].

Different numerical schemes were used for the early-stage evaluation. The numerical schemes play a key role in discretizing the governing physical equations. Fluent offers the second-order upwind implicit ROE scheme with Flux-Difference Splitting [34] (ROE-FDS) based on the Roe scheme that approximates a Riemann solver. ROE-FDS consistently splits fluxes according to their corresponding flux method eigenvalues, making it especially effective for capturing discontinuities such as shocks in the supersonic regime.

In Fluent, the Advection Upstream Splitting Method (AUSM) has also been used. It was applied for sonic boom modeling in previously published works [35,36]. The method breaks down the flux vector into a convective component and a pressure component to accurately capture shock discontinuities without introducing numerical artifacts.

In SU2, the Harten–Lax–van Leer-Contact Riemann solver (HLLC) [37,38] was chosen. It modifies the HLL scheme to restore missing contact and shear waves. The HLLC scheme enables capturing the effects of velocity discontinuities in the transverse direction without adding unnecessary diffusion in regions that have been characterized by turbulent diffusion in the horizontal plane.

The computational mesh was composed of two different regions: an unstructured grid in the proximity of the aircraft designed as a half cylinder, and a structured grid aligned with the Mach angle μ for the remainder part of the domain as visible in Figure 2. Figure 2a highlights the difference between the unstructured and structured domain, while Figure 2b shows the whole computational domain. The numerical elements are hexahedral in the structured domain, tetrahedral in the unstructured zone, and pyramidal to connect the two zones. The total number of elements for the configuration is slightly above 20 million.

As is common in CFD simulations, the ambient pressure field is homogeneous with a constant initial condition for the free-stream pressure. The sonic boom signal, however, which travels from an altitude of several kilometers towards the ground, is also affected by the gradients of sound speed and wind during propagation in the atmosphere. To account for these effects of a non-uniform medium, the far-field propagation is conducted with a different modeling approach, which is described in the following section.

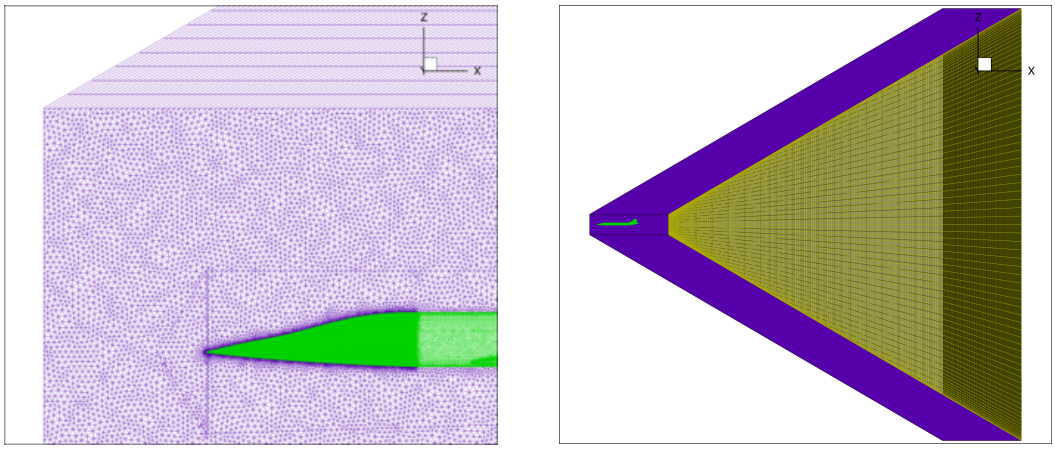

(**a**) (**b**)

Figure 2. Details of the CFD computational domain. (**a**) Unstructured and structured region of the CFD near-field mesh. (**b**) Computational domain of the CFD near-field simulation.

2.1.2. Non-Linear Far-Field Propagation

With increasing radial distance away from the supersonic vehicle, the three-dimensional effects of the fluid motion weaken and the shock waves coming from the different edges of the vehicle merge into one conical shock wave front. As the distance from the aircraft increases, the resulting shock wave front approaches the shape of the Mach cone around the aircraft. With that perspective, the propagation of this Mach cone's shock wave front can now be described with a ray-tracing method. This has the advantage that the refraction of the shock waves due to sound speed and wind gradients can be modeled. While the ray-tracing approach has the disadvantage of assuming locally planar waves (i.e., a far-field assumption), its main advantage is to account for the refraction effects of the stratified atmosphere, which are predominant effects in the far-field regime.

The previously described CFD near-field simulation predicts a pressure distribution around the aircraft which is extracted in parallel to the aircraft's center-line at a radial distance R of one aircraft length $L = 62\,\mathrm{m}$ and at azimuth angles of 0° up to 90° in 10° steps. Symmetry for port and starboard is assumed and was proven by the full CFD simulation, such that extracted pressure signals are mirrored to azimuth angles from −10° to −90°. For the pressure signal extraction, it is more common to use a radial distance of three times the aircraft length ($R/L = 3$), but earlier studies showed a very small impact on the sonic boom predictions for using the lower radial distance of only one aircraft length ($R/L = 1$) in this particular case [18].

The pressure signatures are interpolated on a two-dimensional grid of the location x and the azimuth angle ϕ, such that a smooth transition for azimuth angles between the available input signals is possible. The near-field pressure signals are modified to focus on the shock wave signal and remove unnecessary regions from the CFD solution. This is conducted by transforming the signal from the spatial domain to the Mach cone-aligned normalized variable τ, where $\tau = 0$ represents the tip of the aircraft, and $\tau = 1$ represents the back of the aircraft, regardless of the radial distance r. This is a common normalization for near-field pressure signals in this field. The normalized spatial variable τ also depends on the characteristic length of the aircraft L, the spatial coordinate x, and the Mach angle β according to Equation (1) [39]:

$$\tau = \frac{1}{L}(x - r\beta) \tag{1}$$

The normalized signal is first cut at $\tau_{\mathrm{start}} = -0.2$ and $\tau_{\mathrm{end}} = 1.7$, before a linear fading over the duration of $\tau = 0.2$ at the start and end of the signal is applied to guarantee zero pressure at the signal borders. To make enough space for the non-linear shock wave distortion, the pressure signal is zero-padded to cover the domain from $\tau_{\mathrm{start}} = -1$ until

$\tau_{end} = 2.5$. A similar procedure was used by Park for curating the results of the Second Sonic Boom Prediction Workshop [25]. For the shock wave propagation, the normalized pressure signal from a specific azimuth angle is transformed into the time domain with respect to the aircraft's velocity at each operating condition with a sampling rate of 200 kHz.

The azimuth angle also defines a ray's initial position and orientation on the Mach cone surface. The ray starts on the trajectory point, which is set above the origin of the ground surface plane, with the height being defined by the aircraft's altitude. The orientation of a starting ray is always perpendicular to the Mach cone surface around the aircraft's velocity vector. In this study, the aircraft is always heading towards the east, with a flight path inclination defined by the operating condition. The parameter of variation for the ray tracing is the azimuth angle ϕ. Its orientation is clockwise around the plane's centerline from the pilot's view, with 0° being at the bottom of the aircraft. Thus, the positive azimuth angles are defined towards the aircraft's port side (i.e., left-hand side of the pilot's perspective), and the negative azimuth angles are located at starboard (i.e., right-hand side of the pilot's perspective) as is visualized in Figure 3.

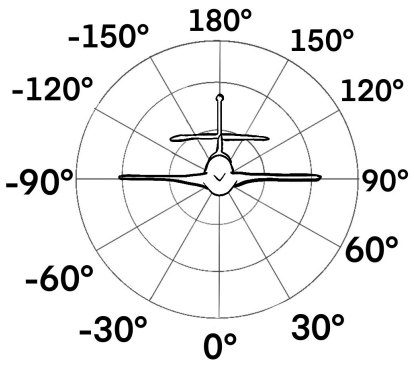

Figure 3. Definition of the ray-tracing azimuth angles ϕ around an aircraft flying towards the reader. Positive azimuth angles are defined towards port side, negative azimuth angles towards starboard side.

As this study solely focuses on primary sonic boom carpets, azimuth angles with a magnitude above 90° are not relevant, as these rays are assumed to only reach the ground as secondary booms, e.g., after being refracted in the thermosphere.

The goal of the ray-tracing simulation is to determine where the shock wave front generated by the aircraft will reach the ground. In a numerical sense, this means finding the azimuth angle region, where rays will hit the ground directly, in contrast to the region of azimuth angles where rays will bend upwards before reaching the ground. With this procedure, the primary sonic boom carpet can be evaluated geometrically. The results are limiting azimuth angles and the geometric position of the ground intersection for every ray. Rays between azimuth angles of $\phi = -40°$ till $\phi = +40°$ are sent out in 10°-steps. Above a magnitude of 40°, rays are sent out every 5°. In addition to this regular azimuth angle array, the limiting azimuth angle is sought with an angle bisection method, and the limiting azimuth angle is rounded to two decimal places. An additional intermediate ray with an azimuth angle between the regular (5° or 10° step) array and the limiting value is analyzed for the present study.

The governing equations for the ray-tracing including wind effects are two-fold. One equation describes the shock wave front position and one equation describes the orientation of the shock wave front normal vector. In a steady medium, i.e., an atmosphere without winds, the orientation of the latter vector would always be perpendicular to the shock wave front. The ray-tracing equations as derived by Onyeonwu [40] and written in a tensor formulation by Yamamoto et al. [41] are as follows:

$$\begin{cases} \dfrac{d\mathbf{R}}{dt} = c_0\mathbf{N} + \mathbf{W} \\ \dfrac{d\mathbf{N}}{dt} = \left(\mathbf{I} - \mathbf{N} \otimes \mathbf{N}^\top\right)\nabla(c_0 - \mathbf{W}\cdot\mathbf{N}) \end{cases} \tag{2}$$

Here, the variable $\mathbf{R}$ represents the position vector of the ray in space. The term c_0 represents the ambient speed of sound, while $\mathbf{N}$ is the unit vector in the direction of the ray's propagation. The vector $\mathbf{W}$ refers to the wind velocity in the atmosphere, which affects the propagation speed of the ray, $\mathbf{I}$ is the identity matrix, and the dyadic product $\mathbf{N} \otimes \mathbf{N}^\top$ constructs a projection operator.

As the ray-tracing approach is a subdivision of geometrical acoustics and only describes the position of waves, but not the amplitude of the wave during propagation itself, a non-linear, one-dimensional wave equation was derived, which accounts for the attenuation and distortion of the shock waves during propagation along ray paths. This equation is referred to as the Augmented Burgers Equation and is described in greater detail in [14,15,41]. The equation is solved in the time domain and does not account for Doppler shifts. However, it accounts for geometrical spreading, a non-uniform atmosphere, non-linear steepening and classical attenuation as well as molecular relaxation. In a dimensional form, the Augmented Burgers Equation can be written as follows [41]:

$$\frac{\partial p}{\partial x} = \frac{\beta}{2\rho_0 c_0^3}\frac{\partial p^2}{\partial t'} - \frac{1}{2A}\frac{\partial A}{\partial x}p + \frac{1}{2\rho_0 c_0}\frac{\partial(\rho_0 c_0)}{\partial x}p + \frac{\delta}{2c_0^3}\frac{\partial^2 p}{\partial t'^2} + \sum_j \frac{(\Delta c)_j \tau_j}{c_0^2}\left(1 + \tau_j\frac{\partial}{\partial t'}\right)^{-1}\frac{\partial^2 p}{\partial t'^2} \tag{3}$$

The variable x represents the spatial coordinate along the propagation direction of the wave. The pressure perturbation due to the sonic boom is denoted by p, representing the acoustic pressure at a given point. The variable t' is a retarded time variable representing the time coordinate in the frame moving with the shock wave, used to account for the delayed arrival of sound due to finite propagation speed.

The parameter c_0 refers to the ambient speed of sound in the atmosphere, while ρ_0 is the ambient air density. The non-linearity coefficient β characterizes the strength of nonlinear effects in the propagation of the shock wave. The term A represents the cross-sectional area of the propagation path, which is driven by the geometric spreading. It is modeled by a four-sided tube which is created with the help of three additional rays with small variations in azimuth angle and source location on the flight trajectory [41]. Additionally, δ represents the diffusivity of sound due to both viscosity and heat conduction. The final summation term accounts for frequency-dependent attenuation and relaxation effects in the medium, where $(\Delta c)_j$ refers to changes in sound speed due to different physical mechanisms, and τ_j is the relaxation time constant for each mechanism.

Equation (3) is solved in the normalized form proposed by Rallabhandi [15] with a split-step algorithm, that solves individual terms independently. The ray-tracing (Equation (2)) uses a first-order Euler method with a step size of $\Delta t = 0.01$ s. This is also the limiting maximum step size for the shock wave propagation, which uses a variable step size, set to one-half of the local shock formation distance. The computation time for a ray including shock wave propagation is in the order of a few minutes on a state-of-the-art notebook, depending on the total length of the ray.

2.2. Simplified Sonic Boom Modeling Approach (Carlson Method)

Carlson developed a useful handbook procedure for the sonic boom calculation of N-wave for a supersonic configuration [17]. The method can evaluate the value of bow shock overpressure, time signature duration, and the extent of the primary carpet. It is a rapid computation method, intended for the early stages of the conceptual design phase. Unlike other approaches, this methodology does not require a large amount of data or needs high computational power, and is valid for all conventional slender supersonic configurations in stationary flight or moderate climb/descent flight phases until 76 km of altitude.

The simplification of the methodology consists of the reformulation of the Whitham F-function [42], which is estimated as a constant called aircraft shape factor K_S. It takes into account the geometrical shape and flight condition of the reference aircraft. For some configurations, there are dedicated charts that allow a rapid computation of the estimated sonic boom characteristics and consist of a numerical representation of the shape factor parameter K_S as a function of the flight conditions.

Besides this approximation, the methodology has numerous limitations for application that go beyond the conceptual design stages; in fact, it is only valid for N-wave booms with an initial compression followed by a linear expansion, and a second shock to return the pressure value to the atmospheric one. Conventional supersonic aircraft have this typology of sonic boom pressure signals on the ground, at least for the bow shock and the positive portion of the signature. However, future civilian supersonic aircraft with specific low-boom designs might have a different shock wave behavior in order to fly in a supersonic regime over land [26,43]. The reference aircraft in the present study does not fall into the low boom category, such that the simplified N-wave assumption is valid.

The first step of assessing the sonic boom generated by a supersonic configuration with this simplified methodology is the evaluation of the equivalent cross-sectional area, which corresponds to the cross-sectional area perpendicular to the Mach cone. A further simplification is the consideration of just the cross-sectional area. This simplification becomes inaccurate for high angles of attack. The area of the air stream tube that is entering the engine inlet should be subtracted from the calculation if it is known.

The following step is the evaluation of the equivalent area due to lift, which can be approximated as the lift planform distribution of the aircraft. It depends on the aircraft weight, the flight path angle, the ray azimuth angle, the aircraft planform area and the local span of the aircraft along the longitudinal axis. The lifting force, which influences the sonic boom, is defined by an aircraft weight component that is normal to the flight path and directed along the initial ray-path azimuth angle.

The third step consists of the combination of the two previously described contributions, to obtain the total effective area of the aircraft. With that, it is possible to evaluate key parameters for the determination of the simplified shape factor constant.

The final terms for the evaluation of bow shock overpressure and time signature duration are weather-related. The methodology includes two different factors for evaluating the atmosphere and the ground, called the pressure amplification factor, which accounts for nonuniform atmospheric effects, and the reflection factor, assumed to be 2.0.

The equations of Carlson's methodology for the evaluation of shock overpressure and time duration are as follows [17]:

$$\Delta p_{\max} = K_p K_R \sqrt{p_v p_g} \left(M^2 - 1\right)^{1/8} h_e^{-3/4} l^{3/4} K_S \tag{4}$$

$$\Delta t = K_T \frac{3.42}{a_v} \frac{M}{\left(M^2 - 1\right)^{3/8}} h_e^{1/4} l^{3/4} K_S \tag{5}$$

Here, $\Delta p_{\max}$ is the bow-shock overpressure and Δt the signature duration. The correction factors K_p, K_R account for different atmospheric and ground effects, K_t is a correction factor for the time duration, and K_S is the aircraft shape factor parameter. The characteristic aircraft length is denoted as l, while M is the Mach number of the vehicle and h_e denotes the effective altitude of the vehicle. The ambient speed of sound is a_v in Carlson's notation and p_v and p_g are the atmospheric and ground pressure terms, respectively.

2.3. Acoustic Parameters and Metrics

As is common in acoustics, a pressure signal can be transformed into a single value, which aims to quantify the annoyance or loudness of the audio event. As annoyance or loudness are not physical quantities, this final transformation of the pressure signal relies

on the knowledge about auditory perception. Findings from psycho-acoustics provide standardized acoustic metrics to depict this final step of hearing [44,45].

As there is still ongoing research on the definition of suitable sonic boom metrics [11,46], the study provides the ground impact of the simulated sonic booms with not only one but a few relevant acoustic metrics, which have shown to correlate with sonic boom annoyance [9] and might be considered for a yet-to-be-defined standard on sonic boom perception. A widely used loudness metric for the sonic boom is Stevens' Perceived Level of Noise Mk VII (PL) [47] which is given in decibels (dB). The PL values in this paper are computed with the open-source Python library PyLdB [48]. Sound Exposure Levels (SEL) with frequency weightings (A, B, C, D) have been shown to correlate with sonic boom annoyance. They are computed according to ISO 1996-1:2016 and are given in dB [49]. Indoor Sonic Boom Annoyance Predictor (ISBAP) is a metric that was derived to correlate with sonic boom annoyance inside buildings. It is a weighted combination of PL, SEL(A) and SEL(C) and is given in dB [50].

The peak amplitude of a sonic boom shock wave is the difference from the highest pressure value in the signal to the ambient pressure, which is also referred to as overpressure. The signal duration of an N-wave, i.e., the typical sonic boom pressure signal on the ground, is defined as the time difference between the signal maximum and minimum.

2.4. Reference Aircraft CS1

The supersonic aircraft represents a modernized version of the Concorde, which was re-designed with a cruise speed of Mach 2 [51] at an altitude of around 18 km and is referred to as "CS1". A detailed description and analysis of the near-field simulations for the reference aircraft can be found in [13]. To scale the vehicle, ASTRID-H was used, which is an in-house design tool of Politecnico di Torino [52], for defining the configuration of an aircraft. The main goal of the re-design was the use of biofuel as a propellant while maintaining the cruise speed of Mach 2. The design process started from a set of design constraints and operational requirements very similar to the reference Concorde aircraft. The final characteristics of CS1 are shown in Table 1.

Table 1. CS1 main characteristics.

Aircraft Parameter	Value
Overall Length [m]	61.7
Wingspan [m]	25.6
Payload Capacity [kg]	15,200
Reference Range [km]	6500
Max. Take Off Mass [kg]	179,850
Operating Empty Mass [kg]	79,460
Design Fuel Mass [kg]	85,289
Wing Surface [m^2]	358

A geometry model of the supersonic aircraft is shown in Figure 4. The aerodynamic behavior was analyzed extensively [51]. A mission analysis verified compliance with the initial requirements. The effects given by the deflection of control surfaces and viscosity were analyzed and validated with engineering equations. The propulsion database was developed with the software tool EcoSimPro 6.4.0. [53] by studying on-design and off-design conditions.

Based on the derived aerodynamic and propulsive database, it was possible to simulate a mission profile that is coherent with the high-level requirements. The commercial software ASTOS 9.0 has been used for the higher-fidelity mission profile [54].

Figure 4. Geometry model of CS1.

The final aircraft concept is capable of covering a mission profile that falls within the requirement imposed in the initial design phase for a generic long-haul flight with an effective range of 6500 km as shown in Figure 5.

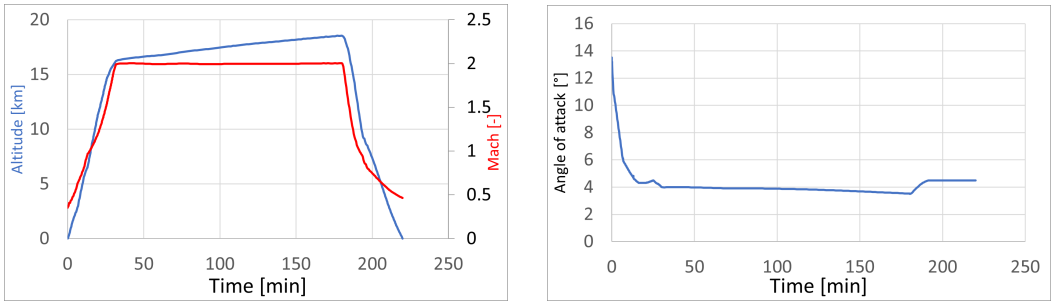

Figure 5. CS1 mission profile and associated Angle of Attack.

The mission connects the cities of Paris and New York. From this realistic flight profile, three reference points were chosen for the sonic boom evaluation. They are labeled "Climb", "Cruise" and "Descent". At those three reference points from the realistic flight trajectory, the parameters Mach number, altitude, angle of attack, and flight path angle are derived. The values are shown in Table 2 and define the test matrix for the subsequent sonic boom analysis.

Table 2. Test Matrix for CS1.

Operating Condition	Mach	Altitude [m]	Flight Path Angle [°]	Angle of Attack [°]
Climb	1.5	15,000	1.15	4.5
Cruise	2.0	18,500	0.02	3.5
Descent	1.5	17,500	−1.17	4.0

All sonic boom modeling approaches in this paper assume a steady state without acceleration. This is an assumption worth noting, as especially during climb and descent, the aircraft is in an accelerated state. For positive acceleration during the climb, focused booms are expected, which would certainly increase the loudness of the generated sonic boom [55]. During the descent phase, the opposite effect is expected. Modeling this focusing or these focusing effects is not performed in this study. As acceleration rates are small at the selected operating conditions, the pure impact of altitude, flight path angle, angle of attack and velocity variation should still indicate meaningful trends, as the comparison of the different operating conditions is the main goal.

2.5. Reference Atmospheres

As the sonic boom is an acoustic phenomenon that occurs for aircraft-induced shock waves traveling many kilometers through the earth's atmosphere to the ground, its intensity on the ground depends on the atmospheric characteristics. In aviation, a common approach to simplifying and standardizing the manifold parameter variations of our atmosphere is the International Standard Atmosphere (ISA) [56]. It defines a vertical temperature profile and a pressure curve, assuming fixed heights and constant temperature gradients for the different atmospheric layers, e.g., troposphere and stratosphere. This definition is not just used to make aviation regulations comparable but also as a standardized layered atmospheric model to derive the formulas used in Carlson's sonic boom prediction approach [17]. Hence, the ISA definition of pressure and temperature was also used for some of the analyses with the higher-fidelity approach.

As humidity has an impact on shock wave attenuation in air, the ISA definition was extended with a standardized humidity profile, according to ANSI S1.26 Annex C [57] as proposed by the organizers of the Sonic Boom Prediction Workshop. This humidity profile is present in the following high-fidelity analyses, even when the atmospheric state is labeled "ISA", while humidity is neglected in the simplified approach.

The International Standard Atmosphere does not define winds, while especially vertical winds can have a major impact on the spreading of the sonic boom shock wave front. For this reason, two atmospheric profiles from measured weather data have been chosen for the study. Choosing a representative atmosphere is a statistical exercise, which has been conducted before. The choice fell on the atmospheric profiles provided for the participants of the Third Sonic Boom Prediction Workshop (SBPW3). To assess sonic boom far-field propagation methods, the organizers selected two atmospheric profiles with specific characteristics from an array of real measured atmosphere profiles over the US [58]. The selected profile used for the first case study of the workshop will be referred to as "SBPW3 Case 1" and reflects on an atmospheric state that leads to a wide range of azimuth angles reaching the ground for an eastward flying aircraft. The second selected profile will be referred to as "SBPW3 Case 2" and refers to an atmospheric state that leads to a particular wide sonic boom carpet for an eastward flying aircraft. For both atmospheres, altitude-dependent temperature, pressure, relative humidity, and horizontal wind speeds are given in tabular format [59,60]. For this study, the values are interpolated with cubic splines, to prevent gradient discontinuities in the simulation domain. The atmospheric profiles are visible in Figure 6. The ground at standard conditions is set to be at an altitude of 0.1 m, and due to the definitions of the realistic profiles, at an altitude of 264.1 m for the SBPW3 cases.

To account for the reflection of the ground, which will also impact the audible event for a listener on the ground, the sonic boom shock wave amplitude is multiplied by a factor of 2. This differs from the definitions of SBPW 3 (which suggests a reflection factor of 1.9) but is in line with the proposed factor by Carlson. However, employing a factor of 2 assumes an ideal planar surface devoid of obstacles and optimal reflection behavior, which simplifies the actual terrain. The influence of realistic topography [61] and the even more pronounced impact of urban canyons [62] has been investigated in a two-dimensional domain, indicating substantial effects on sonic boom perception, which is not considered in this study.

Another important atmospheric mechanism that is neglected in this study is the role of atmospheric turbulence in the planetary boundary layer. The turbulence can have a large impact on the ground signature and introduces variance to the associated sonic boom loudness [11,63].

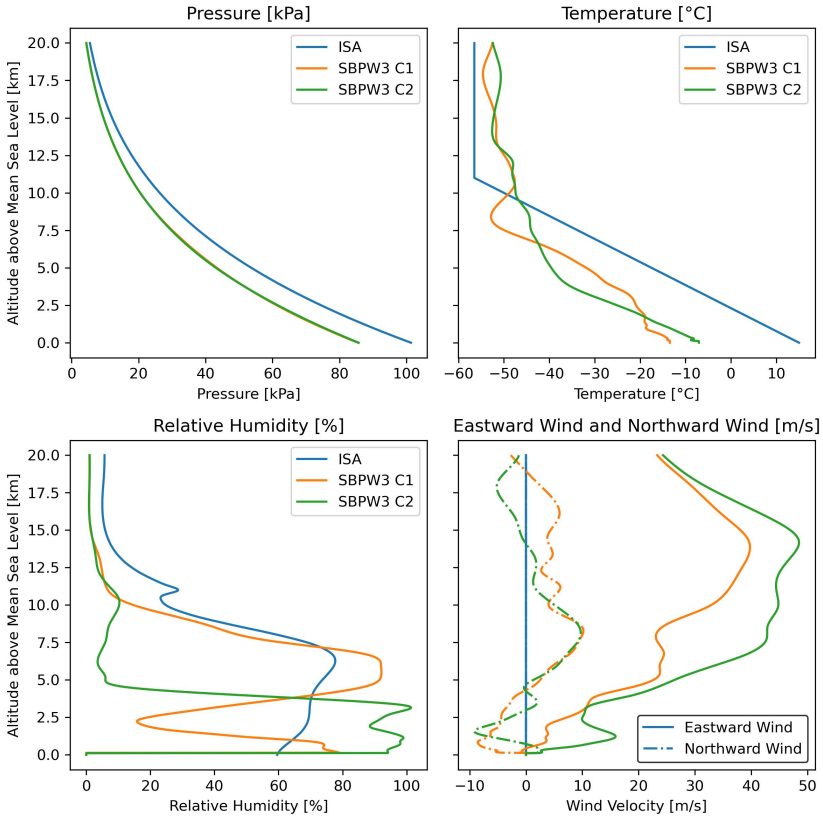

Figure 6. Properties of the three reference atmospheres for the current study. The pressure profiles of both cases of SBPW3 are almost identical, such that the orange line is hidden by the green one in the pressure plot. The wind velocities in both directions are zero for the windless ISA case.

3. Results

As the simplified method has fewer input parameters and results, the predictions of the Carlson method are presented first. Afterward, the results of the higher-fidelity method are showcased, and finally, the comparison of the results of both prediction methods is presented.

3.1. Simplified Method Predictions (Carlson Method)

Applying Carlson's method as described in Section 2.2 gives an array of peak amplitudes and signal lengths for the predicted, idealized sonic boom N-wave on the ground. The computed peak overpressures and signal duration are displayed in Table 3. The operating condition describes the aircraft's state during supersonic operation as defined in Table 2. The N-wave parameters are computed for azimuth angles ϕ, ranging from 0° to 50°. As winds are neglected in this procedure, the results can be mirrored to the opposite lateral direction, i.e., negative azimuth angles.

During the climb, which is evaluated at the lowest altitude (15,000 m) of the three operating conditions, the predicted N-waves on the ground have the highest amplitude and the shortest signal duration in comparison to the other two, with an on-track peak over-pressure of 104.5 Pascal for an N-wave signal of 194.1 milliseconds duration.

The lowest peak amplitudes (e.g., 79.7 Pa at an azimuth angle of 0°) are obtained during cruising, which has the highest altitude (18,500 m) and the highest Mach number of the three conditions. In comparison to the predictions for the descent case, the cruise N-wave signals have a slightly shorter duration. With an on-track signal length of 201.8 ms, they are still longer than those predicted for the lower and slower climb conditions. Regardless of the operating condition, increasing the off-track angle always leads to decreasing amplitudes and increasing signal duration.

Table 3. Carlson method predictions for sonic boom N-wave parameters on ground for the three previously described operating conditions and azimuth angles from 0° to 50°.

Operating Condition	Azimuth Angle [°]	Peak Amplitude [Pa]	Signal Duration [s]
Climb	0	104.5	0.1941
	10	102.3	0.1949
	20	94.3	0.1962
	30	85.5	0.1985
	40	75.2	0.2035
	50	61.1	0.2086
Cruise	0	79.7	0.2018
	10	78.1	0.2029
	20	72.2	0.2048
	30	65.4	0.2084
	40	56.6	0.2124
	50	45.0	0.2188
Descent	0	85.6	0.2045
	10	84.1	0.2056
	20	77.9	0.2084
	30	70.6	0.2114
	40	61.2	0.2168
	50	48.0	0.2234

3.2. Higher-Fidelity Predictions

Due to the two-domain separation of the far-field propagation method (Section 2.1) it is possible to represent different stratified atmospheric profiles during sonic boom prediction. For this reason, computation results are displayed for the International Standard Atmosphere (ISA) definition, which aims to be close to the assumptions of the simplified approach, as well as for two realistic atmospheric profiles from the Third Sonic Boom Prediction Workshop (SBPW3). All three atmosphere models are described in Section 2.5. The intention is to give an insight into the impact of realistic atmospheric conditions on sonic boom behavior.

3.2.1. Near-Field Simulation

The distinct computational fluid dynamics (CFD) domain allows for a detailed analysis of the supersonic flow mechanisms in the proximity of the aircraft, which enables the analysis of variations in the angles of attack and more versatile modeling of different free stream pressures and velocities. It also gives a detailed insight into the azimuth directivity behavior of the shock waves generated in the supersonic flow. From the CFD solution, pressure signals are extracted at different azimuth angles to be used as an input for the non-linear far-field propagation and to link the two simulation domains of the higher-fidelity sonic boom modeling approach. Some examples of the extracted pressure signals are shown in Figure 7. The generation of the near-field results is described extensively in [13], while this study focuses more on the far-field prediction results.

The left plot of Figure 7 depicts the pressure signature for the on-track condition directly below the aircraft. The differences between the climb, cruise, and descent pressure signals are solely introduced through the different angles of attack and the different free-stream conditions in the CFD near-field simulation.

The first small peak of the pressure signals depicts the shock wave generated by the nose of the aircraft, while the dominant peak can be associated with the shock waves generated from the wing surface. After the overpressure shocks have passed the observer, a relaxation leads to an area of negative acoustic pressure before the acoustic pressure returns to zero. As both subplots show extracted pressure signals from below the aircraft, the regions of positive overpressure predominate the signal due to the lift of the aircraft generating an overpressure below the aircraft.

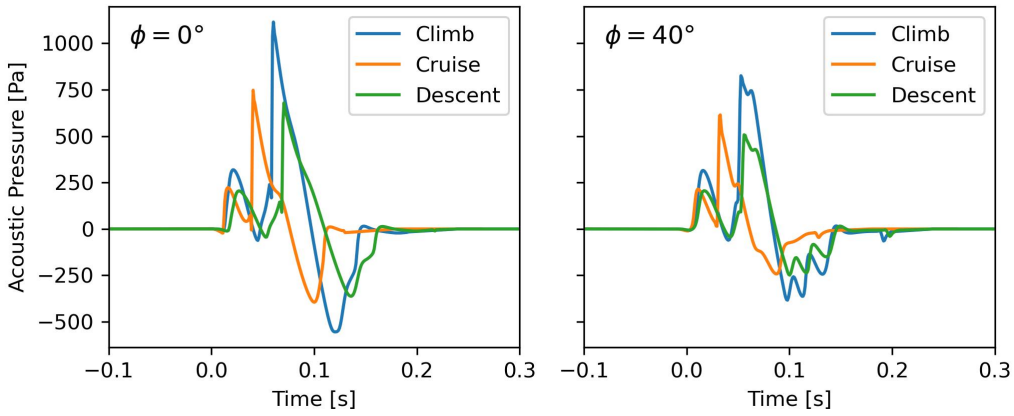

Figure 7. Extracted near-field pressure signatures from the CFD solution at a radial distance of $R = 1L = 62\,\text{m}$ for the three operating conditions of CS1. The azimuth angle of $\phi = 0°$ shows the extracted pressure signal below the aircraft (on-track). The right plot shows an exemplary pressure signature extracted at off-track conditions for an azimuth angle of $\phi = 40°$.

This also explains why at the climb condition, i.e., at the condition with the highest angle of attack (and thus highest lift) plus a low altitude with the highest ambient pressure, the highest amplitude for the three compared near-field shock waves occurs. The cruise condition has the highest Mach number (Mach 2.0 for cruise vs. Mach 1.5 for climb and descent) and results in the shortest signal duration, as the aircraft passes an observer with higher speeds, and thus, the duration of the acoustic event is shorter for that observer. The comparison of cruise and descent conditions, which are at similar altitudes and similar angles of attack, reveals that the influence of velocity is mostly reflected in the signal duration but barely in the peak amplitudes.

The same trends can be observed in the right-hand side plot, which shows the extracted pressure signature at an azimuth angle of 40°. In general, the overall amplitudes are smaller for all operating conditions at this off-track azimuth angle, as the lift created from the wing surfaces is less present in this direction. Here, an influence of the higher velocity during cruise can be seen, as the dominant peak has formed a full shock spike, while the equivalent shock waves at climb and cruise have not yet merged completely into such a sharp shock spike.

3.2.2. Ray Tracing

To simulate the sonic boom on the ground, the first step of the higher-fidelity far-field approach is a ray tracing algorithm to account for the refraction of the non-uniform atmosphere, as described in Section 2.1.2.

The geometric position of the sonic boom footprint for CS1 flying towards the east in the different atmospheric models is plotted in Figure 8. The limiting azimuth angles of the primary sonic boom carpet are labeled in the figure and printed in Table 4. For the standard atmosphere without winds, the direction of the aircraft has no impact on the lateral throw, but rounding errors due to different handling of signed floating point numbers are observed in some cases. The windy atmospheric profiles of the Third Sonic Boom Prediction Workshop were selected for an eastwards heading aircraft, such that we stick to this definition to make use of the known properties of those two atmospheres. This leads to the port-side lateral throw going towards the north and the starboard-side lateral throw going towards the south.

The most obvious influence on the geometric behavior of the sonic boom carpet comes from the higher Mach number of the cruise condition. Due to the higher Mach number, the Mach cone is sharper and thus, the rays (starting perpendicular to the Mach cone) have a lower degree towards the front of the aircraft. This results in a lower frontal throw and a wider lateral throw for rays reaching the ground.

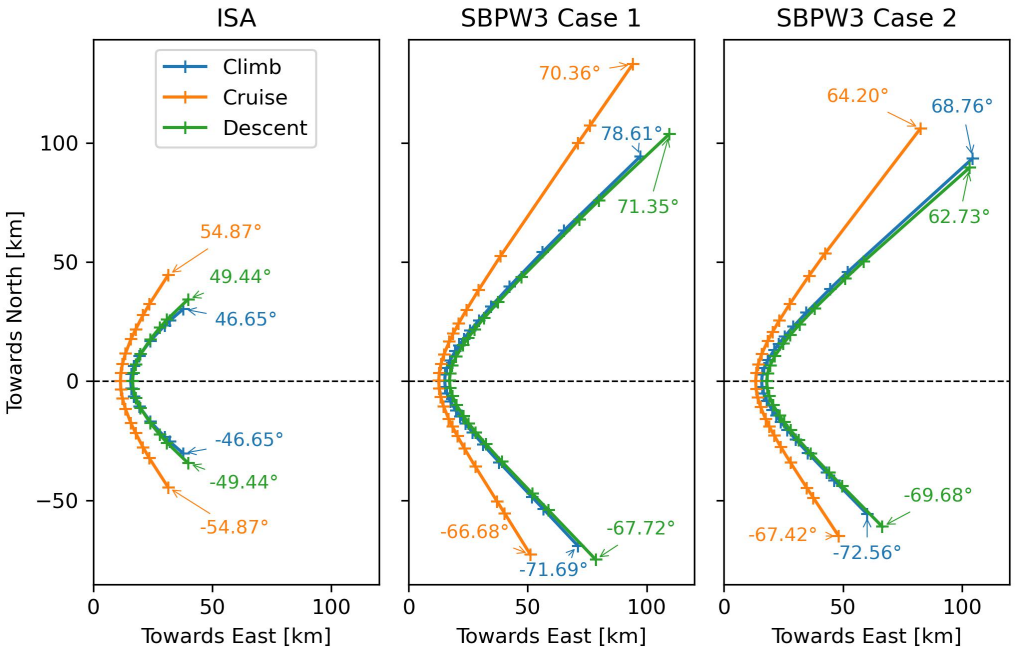

Figure 8. Computed primary sonic boom footprint for CS1 flying towards east. The marks depict the ground intersection points of the computed rays. The labels show the values of the limiting azimuth angles ϕ. **ISA** shows the footprint in the windless International Standard Atmosphere, **SBPW3 Case 1** for the realistic atmosphere from the Third Sonic Boom Prediction Workshop (SBPW3) with a wide range of azimuth angles, and **SBPW3 Case 2** the SBPW3 case for a realistic atmosphere that is intended to result in a particular wide carpet.

Table 4. Geometric Parameters of the Sonic Boom Carpet for Different Atmospheres and Operating Conditions.

Atmosphere	Operating Condition	Min. Azimuth Angle [°]	Max. Azimuth Angle [°]	Starboard Lateral Throw [km]	Port Side Lateral Throw [km]	Carpet Width [km]	Frontal Throw [km]
ISA	Climb	−46.65	46.65	30.3	−30.3	60.5	37.8
	Cruise	−54.87	54.87	44.6	−44.5	89.1	31.4
	Descent	−49.44	49.44	34.4	−34.4	68.8	39.8
SBPW3 Case 1	Climb	−71.69	78.61	94.3	−69.1	163.4	97.3
	Cruise	−66.68	70.36	133.1	−72.7	205.8	94.1
	Descent	−67.72	71.35	103.8	−74.9	178.7	109.6
SBPW3 Case 2	Climb	−72.56	68.76	93.6	−55.8	149.4	104.5
	Cruise	−67.42	64.20	106.1	−65.0	171.1	82.6
	Descent	−69.68	62.73	89.7	−61.1	150.8	103.2

For the realistic atmospheres with winds, the geometric carpet of the aircraft flying towards the east extends significantly. Towards the port side (i.e., towards the north) the lateral throw in the windy atmosphere is around three times higher than that in the standard atmosphere. It has to be highlighted once more that these are extreme cases from a set of measured atmospheric profiles, to achieve a particularly wide range in azimuth angles in case 1, and a particularly wide carpet width in case 2 (see Section 2.5). These expected trends are visible in the obtained results, although in the present study, the first case of the sonic boom prediction workshop leads to an even wider carpet than case 2. As the flight altitude in the SBPW3 examples differs from the ones used here, atmospheric winds can have a different effect on the ray paths. Thus, the intended behavior for the

case studies of the Third Sonic Boom Prediction Workshop does not necessarily have to be reproduced in the current study.

While the geometric sonic boom footprint during the climb is a little ahead of the footprint at descent conditions in the standard atmosphere, the opposite behavior is observed with the realistic atmospheric profiles. Except for the standard atmosphere, the widest range of azimuth angles is always observed for the climb condition, although the lateral throw of the descent condition is usually wider than the one of the climb. The only exception for this behavior is the northward throw at SBPW3 Case 2. In this extreme case, the rounding towards 2 decimal places might be too coarse as even smaller variations of the azimuth angle have shown to have a great impact on the final lateral throw, specifically in this atmosphere.

While this imposes a challenge for the definition of the geometric extent of the sonic boom carpet, the following chapters will show that the sound intensity reaching these far outside areas is negligible (see Section 3.2.4).This means that higher-resolution ray-tracing steps are not necessary for the goal of defining an acoustic sonic boom carpet.

3.2.3. Pressure Signals on Ground

Along the analyzed and previously described rays, the near-field signatures from the CFD solution are propagated toward the ground. The resulting signature for the on-track ray at an azimuth angle of $\phi = 0°$ in the standard atmosphere is depicted in Figure 9, alongside the ground signature of $\phi = 40°$. This is, in a sense, the direct output of the far-field propagation algorithm for the input near-field signatures from Figure 7 when applying the International Standard Atmosphere. All the shocks have coalesced into one overpressure shock at the beginning and one expansion shock at the end of the signal. This observation due to the non-linear steepening of sonic boom is referred to with the label "N-wave" of conventional sonic booms.

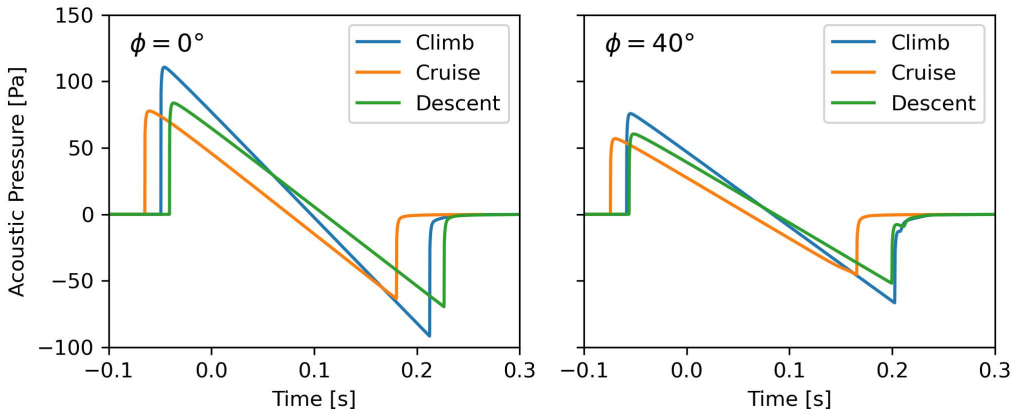

Figure 9. Computed shock wave pressure signatures at ground level for the three operating conditions of CS1 in the International Standard Atmosphere. The azimuth angle of $\phi = 0°$ shows the on-track sonic boom and the right plot shows an exemplary off-track sonic boom, computed for an azimuth angle of $\phi = 40°$.

The amplitude of the first shock and the signal duration between the bow and aft shock are the parameters that are also estimated by Carlson's method. For the higher-fidelity method, those parameters are evaluated from the computed signatures for the different operating conditions, atmospheres and azimuth angles. The obtained values can be found in Table 5.

Figure 10 shows the results for the input pressure signals of Figure 7 when applying the realistic atmosphere profiles from SBPW3. The differences in the predicted sonic boom on the ground between the two realistic atmosphere profiles are marginal. The off-track amplitudes and signal duration are usually smaller than the ones on-track. The peak amplitudes of the N-waves in any of the measured SBPW3 atmosphere cases are generally smaller than the predicted N-wave in the standard atmosphere (Figure 9), but the shape of the shock wave also coalesced into an almost ideal N-wave.

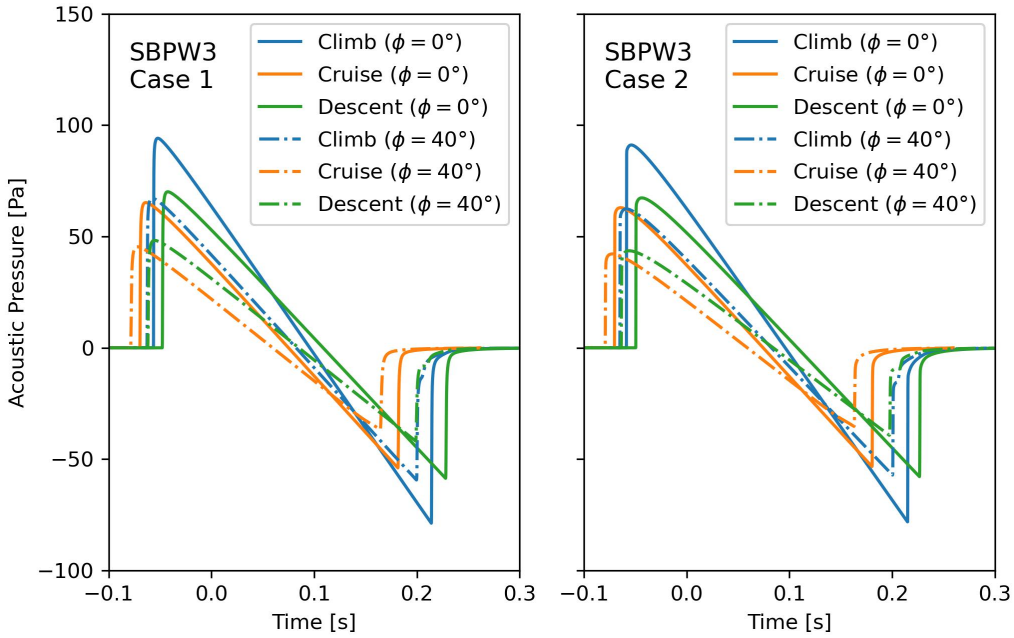

Figure 10. Computed shock wave pressure signatures at ground level for the three operating conditions of CS1 in the realistic atmospheres of the Third Sonic Boom Prediction Workshop (SBPW3). The left plot depicts case 1 and the right plot depicts case 2. The azimuth angle of $\phi = 0°$ is plotted with solid lines. Dash-dotted lines show an exemplary off-track sonic boom at an azimuth angle of $\phi = 40°$.

3.2.4. Acoustic Sonic Boom Carpets

The final exercise of the higher-fidelity prediction is the transformation of the predicted shock wave on the ground into an acoustic metric to quantify the annoyance or loudness of the sonic boom for listeners in the region of the sonic boom carpet. As there is no standardized sonic boom annoyance metric at the moment, a couple of promising metrics are computed in parallel. Stevens' Mk VII Perceived Level of Noise (PL) is a widely used loudness metric to describe sonic boom, which is selected as an example to showcase the trends for acoustic levels.

As all simulations and computations are under the cruise assumption, which in this case means the aircraft is in a steady state without acceleration during all its operating conditions, the frontal throw has a low practical relevance. The exact time when the sonic boom occurs does not really have an impact on its annoyance, and the supersonic aircraft would sooner or later cause a sonic boom at all positions inside the lateral limits of the sonic boom carpet when passing an observer on the ground. Thus, the definition of the acoustic sonic boom carpet for a steadily fling aircraft relies only on the lateral throw and the observed shock wave on the ground. Figure 11 depicts this lateral acoustic sonic boom carpet.

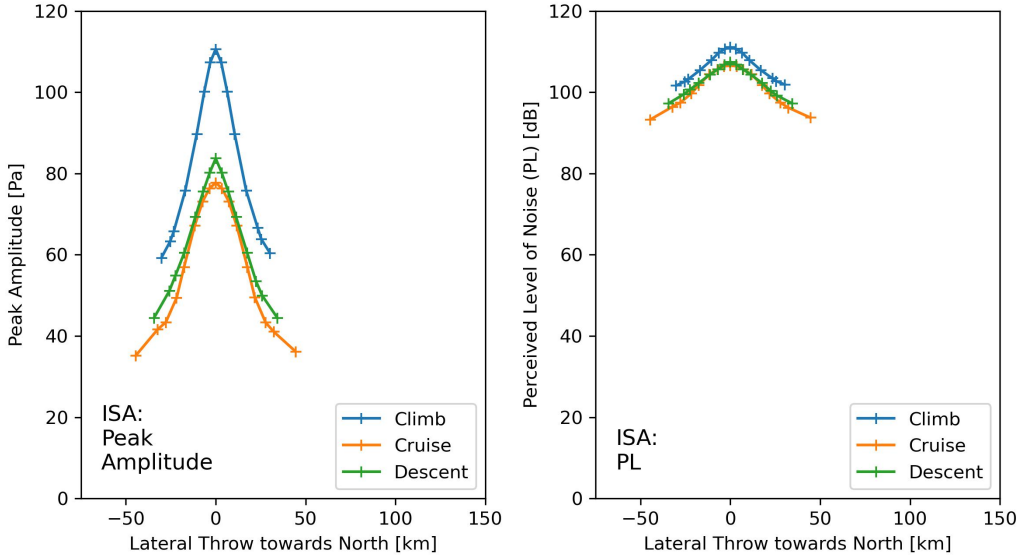

Figure 11. Computed acoustic sonic boom carpet as observed at ground level for the three operating conditions of CS1 flying towards east (i.e., towards the reader) in the International Standard Atmosphere. The left plot shows the distribution of peak amplitudes over the sonic boom carpet, and the right plot shows the distribution of Stevens' Perceived Level of Noise Mk VII.

The left subplot shows the peak amplitudes at the computed impact points (marked with plus signs) over the lateral throw of a supersonic aircraft flying in the direction of the reader. Its trajectory is located at the operation-specific altitude above the origin of the x-axis. The plot shows, how the peak amplitude of the sonic boom changes, depending on the lateral position below the trajectory. The result in this figure was computed for the International Standard Atmosphere, and the (lateral) carpet width is the same as for the ISA case in Figure 8. The new information in this plot is the quantification of the shock wave on the ground, such that it shows the maximum peak amplitude (directly below the trajectory), the minimum observed peak amplitude (at the edges of the primary sonic boom carpet), and the distribution of peak amplitudes in between.

The right-hand side subplot shows the associated PL values of the computed ground signals, such that the plotted curves correlate more with the human perception of the shock wave. An overview of the values of the acoustic sonic boom carpet is shown in Table 5. It is worth noting that the rounding errors are due to different floating point precision handling in the positive and negative domain for the off-track angles. As there are no winds present in this atmosphere model, full symmetry is otherwise expected. In both plots, the most significant feature is the higher amplitude and loudness during the climb phase. The maximum loudness is achieved directly below the trajectory, but is still on a high level at off-track positions inside the carpet limits, as the PL values remain higher than 90 dB over the full carpet width and under all conditions, which can be considered as "loud" by all means.

Figure 12 shows the acoustic sonic boom carpet in the atmosphere from the first case of SBPW3. It allows for assessing the acoustic properties of the sonic boom carpet in this realistic atmosphere with winds. Also, in this case, the peak amplitude and loudness on the ground are significantly higher during the climb phase compared to the other operating phases. Even when just looking at impact points with a Perceived Level of Noise above 80 dB, the carpet in this windy atmosphere spreads wider than under standard conditions. However, at the limiting azimuth angles, a significant decrease in the PL values is observed. It is from around 60–70 dB at a lateral offset of around 75 km towards the south and around 20–30 dB in the northern cutoff region. For the northern spread, the cruise condition results in a significantly wider lateral spread at even higher loudness values. While the climb

and descent are cut off at around 100 km towards the north, the sonic boom of the cruise condition cuts off at around 130 km.

Table 5. N-wave parameters at different azimuth angles for the three operating conditions in ISA atmosphere.

Operating Condition	Azimuth Angle [°]	Lateral Throw Towards North [km]	Peak Amplitude [Pa]	Signal Duration [s]	Perceived Level of Noise (PL) [dB]
Climb	−46.65	−30.3	59.2	0.2706	101.6
	−40.00	−17.0	75.8	0.2570	105.4
	0.00	0	110.6	0.2582	111.1
	40.00	17.0	75.8	0.2570	105.4
	46.65	30.3	60.4	0.2709	101.9
Cruise	−54.87	−44.5	35.1	0.2489	93.3
	−40.00	−17.6	56.9	0.2348	101.7
	0.00	0.0	77.7	0.2403	106.6
	40.00	17.6	56.9	0.2348	101.7
	54.87	44.6	36.1	0.2498	93.7
Descent	−49.44	−34.4	44.4	0.2591	97.2
	−40.00	−17.5	60.4	0.2510	102.3
	0.00	0.0	83.7	0.2630	107.5
	40.00	17.5	60.4	0.2510	102.3
	49.44	34.4	44.4	0.2590	97.2

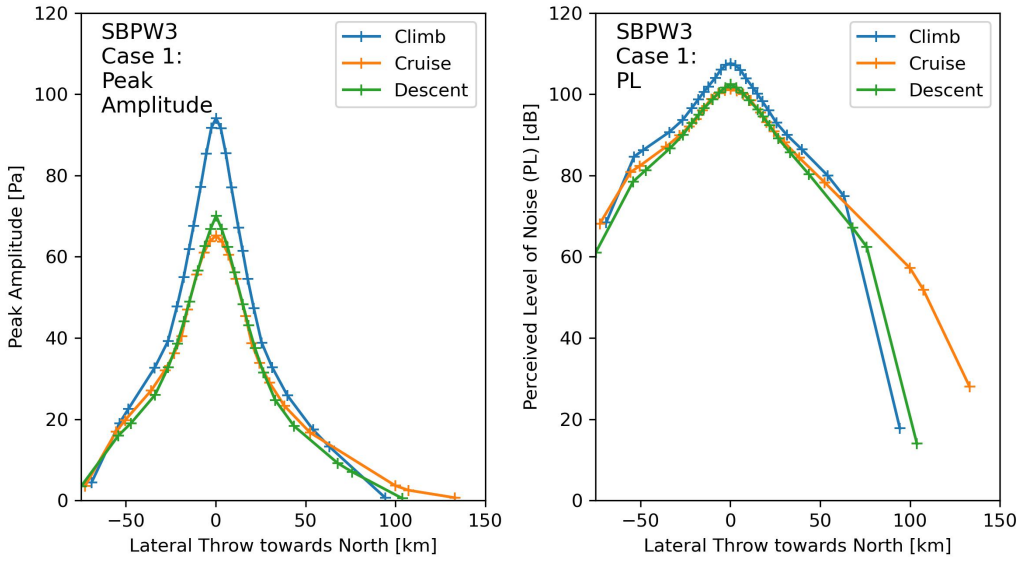

Figure 12. Computed sonic boom carpet at ground level for the three operating conditions of CS1 flying towards east in the first realistic atmosphere of SBPW3. The left plot shows the distribution of peak amplitudes over the sonic boom carpet, and the right plot shows the distribution of Stevens' Perceived Level of Noise Mk VII.

The values of the plotted behavior can be found in Table 6.

Table 6. N-wave parameters at different azimuth angles for the three operating conditions in SBPW3 Case 1 atmosphere.

Operating Condition	Azimuth Angle [°]	Lateral Throw Towards North [km]	Peak Amplitude [Pa]	Signal Duration [s]	Perceived Level of Noise (PL) [dB]
Climb	−71.69	−69.1	4.4	0.2811	68.4
	−40.00	−12.4	67.5	0.2560	101.9
	0.00	0.2	94.1	0.2662	107.6
	40.00	12.6	67.2	0.2570	101.6
	78.61	94.3	0.7	0.2659	17.8
Cruise	−66.68	−72.7	3.6	0.2529	68.1
	−40.00	−15.8	47.0	0.2365	96.1
	0.00	0.2	65.2	0.2454	101.3
	40.00	16.6	45.4	0.2363	95.5
	70.36	133.1	0.7	0.2245	28.1
Descent	−67.72	−74.9	3.5	0.2708	61.1
	−40.00	−14.7	48.9	0.2533	96.5
	0.00	0.2	70.1	0.2703	102.4
	40.00	15.1	48.2	0.2540	96.2
	71.35	103.8	0.5	0.2627	14.0

For the third atmospheric model, the second defined case of SBPW3, the previously described trends can be observed as well, as shown in Figure 13. The climb condition results in the highest peak and loudness on the ground and the carpet width for this windy condition is generally wider than for the standard atmosphere. The cruise condition results in louder sonic booms near the edges of the carpet.

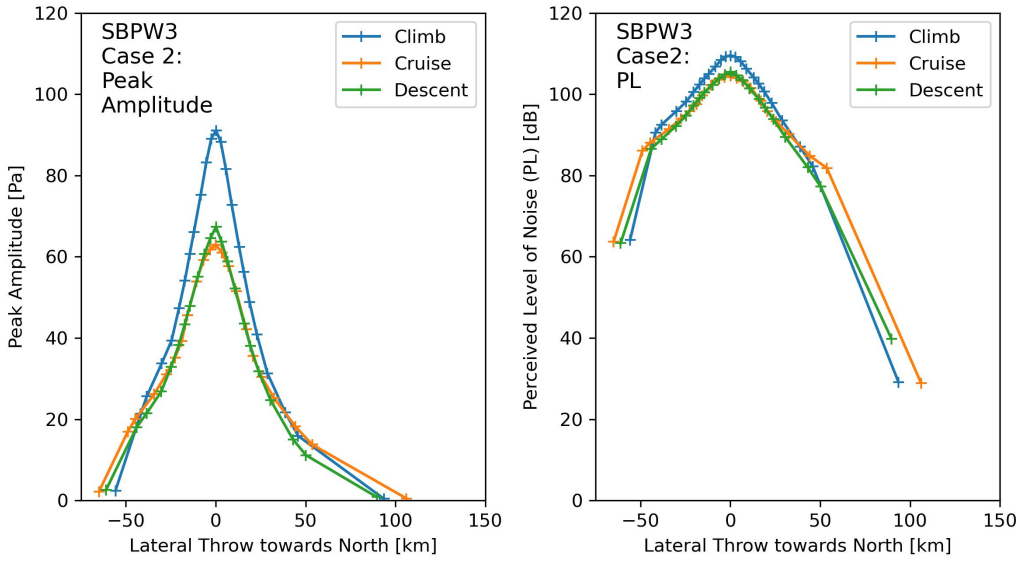

Figure 13. Computed sonic boom carpet at ground level for the three operating conditions of CS1 flying towards the east in the second realistic atmosphere of SBPW3. The left plot shows the distribution of peak amplitudes over the sonic boom carpet, and the right plot shows the distribution of Stevens' Perceived Level of Noise Mk VII.

The most relevant values are printed in Table 7.

Table 7. N-wave parameters at different azimuth angles for the three operating conditions in SBPW3 Case 2 atmosphere.

Operating Condition	Azimuth Angle [°]	Lateral Throw Towards North [km]	Peak Amplitude [Pa]	Signal Duration [s]	Perceived Level of Noise (PL) [dB]
Climb	−72.56	−55.8	2.4	0.2757	64.2
	−40.00	−12.1	66.1	0.2589	105.0
	0.00	0.2	91.1	0.2689	109.5
	40.00	13.0	62.4	0.2591	104.1
	68.76	93.6	0.4	0.2551	29.1
Cruise	−67.42	−65.0	2.2	0.2486	63.7
	−40.00	−15.8	45.6	0.2361	99.7
	0.00	0.1	62.9	0.2446	104.5
	40.00	16.9	42.2	0.2351	98.4
	64.20	106.1	0.5	0.2020	28.9
Descent	−69.68	−61.1	2.6	0.2659	63.3
	−40.00	−14.4	47.9	0.2535	100.4
	0.00	0.1	67.3	0.2702	105.5
	40.00	15.8	43.6	0.2531	98.8
	62.73	89.7	0.8	0.2404	39.8

3.2.5. Sonic Boom Characterization with Different Acoustic Metrics

The values at an azimuth angle of $\phi = 0°$ have the shortest distance to the ground associated with the highest near-field peak pressures. For windy atmospheres, this azimuth angle can have an offset from the flight path position of a few hundred meters, which is negligible in relation to the carpet widths in the order of more than 50 km. Therefore, it seems reasonable to assume that the results for the 0° azimuth angle represent the maximum peak pressure and the maximum loudness. With this assumption, an analysis of the upper limits of the sonic boom carpet created by the reference aircraft is an easy task and might give the most comprehensive characterization of the vehicle's sonic boom carpet in the form of an upper boundary for its predictions.

The expected maximum value for the aircraft under the studied conditions is shown in Table 8. This table aims at providing additional results by providing different acoustic metrics (see Section 2.3) and could be re-used if one of those metrics is selected for the definition of future sonic boom regulations. Apart from that, a striking take-away for readers without an acoustic background could be the fact that all the acoustic metrics are given in dB, which is not a unit, but an indicator that the associated value is a (sometimes acoustic) level with respect to some reference value. Stating any number with the "unit" dB does not quantify the value without a statement on the metric or the reference value in use.

Table 8. Acoustic metrics for the maximum sonic boom on ground at an azimuth angle of $\phi = 0°$ for the different atmospheres and operating conditions.

Atmosphere	Operating Condition	PL [dB]	SEL(A) [dB]	SEL(B) [dB]	SEL(C) [dB]	SEL(D) [dB]	ISBAP [dB]	Peak Amplitude [Pa]
ISA	Climb	111.1	95.9	102.2	109.6	102.9	116.8	110.6
	Cruise	106.6	92.2	98.8	106.5	99.2	112.6	77.7
	Descent	107.5	92.9	99.5	107.2	99.9	113.5	83.7
SBPW3 Case 1	Climb	107.6	93.0	100.4	108.1	100.3	114.0	94.1
	Cruise	101.3	87.4	96.3	104.7	96.0	108.6	65.2
	Descent	102.4	88.5	97.1	105.4	96.9	109.5	70.1

Table 8. *Cont.*

Atmosphere	Operating Condition	PL [dB]	SEL(A) [dB]	SEL(B) [dB]	SEL(C) [dB]	SEL(D) [dB]	ISBAP [dB]	Peak Amplitude [Pa]
SBPW3 Case 2	Climb	109.5	95.0	100.9	108.0	101.5	115.0	91.1
	Cruise	104.5	90.7	97.4	104.8	97.4	110.4	62.9
	Descent	105.5	91.6	98.0	105.4	98.2	111.3	67.3

3.3. Comparison of the Prediction Methods

Finally, the predictions of the simplified method as presented in Table 3 and the equivalent predictions of the higher-fidelity method as presented in the tables of the previous section (Tables 5–7) are compared. To assess the validity of the Carlson method for the different operating conditions and different atmospheres, the deviation of peak pressure predictions and signal duration is computed according to Equations (6) and (7).

$$\Delta P_i = P_{Carlson} - P_i \tag{6}$$

and

$$\Delta T_i = T_{Carlson} - T_i \tag{7}$$

with $P_{Carlson}$ and $T_{Carlson}$ being the predicted peak overpressure and signal duration by Carlson, and P_i and T_i being the higher-fidelity's peak pressure and signal duration predictions, respectively. The results are presented in Table 9 and provide a comprehensive comparison of the differences between the simplified Carlson method and high-fidelity sonic boom predictions for three atmospheric conditions: ISA, SBPW3 Case 1, and SBPW3 Case 2. The table highlights the deviations in peak amplitude and signal duration across a range of azimuth angles for each operating condition (climb, cruise, and descent).

Table 9. Deviations of the Carlson predictions from the higher fidelity prediction. ΔP shows the deviation in peak amplitude and ΔT shows the deviation in signal duration.

Operating Condition	Azimuth Angle [°]	ΔP_{ISA} [Pa]	ΔT_{ISA} [s]	$\Delta P_{SBPW3,C1}$ [Pa]	$\Delta T_{SBPW3,C1}$ [s]	$\Delta P_{SBPW3,C2}$ [Pa]	$\Delta T_{SBPW3,C2}$ [s]
Climb	0	−6.1	−0.0641	10.4	−0.0721	13.4	−0.0748
	10	−5.0	−0.0630	10.7	−0.0709	14.0	−0.0734
	20	−5.8	−0.0601	8.8	−0.0667	12.7	−0.0688
	30	−4.2	−0.0561	8.5	−0.0602	12.7	−0.0624
	40	−0.6	−0.0536	8.0	−0.0535	12.8	−0.0556
Cruise	0	2.0	−0.0385	14.5	−0.0311	16.8	−0.0303
	10	1.8	−0.0372	14.4	−0.0297	17.1	−0.0290
	20	−0.9	−0.0337	11.7	−0.0268	14.6	−0.0259
	30	−1.7	−0.0301	10.8	−0.0243	13.9	−0.0232
	40	−0.3	−0.0225	11.2	−0.0160	14.4	−0.0148
	50	1.7	−0.0200	8.9	−0.0082	8.9	−0.0072
Descent	0	1.9	−0.0585	15.5	−0.0658	18.3	−0.0657
	10	3.9	−0.0494	17.3	−0.0565	20.4	−0.0562
	20	2.4	−0.0442	15.5	−0.0508	19.0	−0.0502
	30	1.3	−0.0387	14.4	−0.0442	18.4	−0.0434
	40	0.8	−0.0342	13.0	−0.0372	17.6	−0.0363

For the ISA atmosphere, the simplified methodology generally under-predicts the peak amplitudes during the climb, with percentage differences ranging from −5.5% at 0° to −0.8% at 40°. This under-prediction is notably consistent, showing a systematic deviation in amplitude estimation. The signature duration also shows significant discrepancies, with reductions ranging from −24.8% at 0° to −20.8% at 40°. In contrast, for the cruise and

descent conditions, the percentage deviations for peak amplitudes fluctuate, indicating a less systematic trend. The signal duration differences remain negative throughout, highlighting that the Carlson method consistently predicts shorter sonic boom durations compared to the high-fidelity model.

In the SBPW3 Case 1 atmosphere, the Carlson method shows a notable over-prediction of peak amplitudes across all azimuth angles and operating conditions. The peak amplitude deviations are particularly pronounced during cruise and descent, with maximum deviations reaching up to 25.9% and 27.0%, respectively. This suggests that the simplified approach overestimates the effect of the atmospheric profile on the sonic boom intensity for more complex atmospheric scenarios. Signal duration discrepancies are also significant, ranging from −27.1% to −20.8% for climb and −24.3% to −14.6% for descent. This systematic underestimation indicates a consistent limitation of the Carlson method in accurately capturing the signal duration when the atmospheric conditions deviate significantly from the ISA standard.

The deviations for SBPW3 Case 2 further demonstrate the sensitivity of the simplified methodology to atmospheric complexity. Peak amplitude differences during climb and descent exhibit high positive deviations, reaching up to 20.5% and 40.4%, respectively, indicating substantial over-predictions. The cruise condition follows a similar trend with peak amplitude deviations increasing with azimuth angle. The signal duration deviations, while smaller in magnitude compared to peak amplitudes, still range between −27.8% and −21.5% for the climb and −24.3% and −14.3% for the descent. This consistent pattern suggests that the simplified method's inability to capture complex atmospheric effects is amplified under more extreme scenarios like SBPW3 Case 2.

4. Discussion

The insights gained from comparing sonic boom predictions using both simplified and high-fidelity methodologies highlight their respective strengths and limitations. The results suggest that the Carlson method generally provides a reasonable first estimate of sonic boom characteristics for the selected supersonic operating conditions, i.e., climb, cruise, and descent (see Table 2). While high-fidelity modeling is required for precise and context-specific evaluations, the simplified method effectively captures broad trends related to flight phases and off-track sonic boom behavior. As shown in Table 10, deviations between the simplified and high-fidelity methods remain within a manageable range in an International Standard Atmosphere (ISA). Although the simplified methods fail in predicting sonic boom under realistic atmospheric conditions including winds, the simplified predictions provide at least a conservative over-prediction of peak amplitudes for those cases, as the higher-fidelity method indicated lower peak amplitudes and loudness levels under those conditions.

Table 10. Percentage deviations of peak amplitude and signal duration predictions of the simplified Carlson method in comparison to the higher-fidelity predictions. ΔP is the difference in peak amplitude and ΔT the difference in signal duration.

Operating Condition & Azimuth Angle	ΔP_{ISA} [%]	ΔT_{ISA} [%]	$\Delta P_{SBPW3,C1}$ [%]	$\Delta T_{SBPW3,C1}$ [%]	$\Delta P_{SBPW3,C2}$ [%]	$\Delta T_{SBPW3,C2}$ [%]
Climb: 0°	−5.5	−24.8	11.1	−27.1	14.7	−27.8
Climb: 40°	−0.8	−20.8	11.9	−20.8	20.5	−21.5
Cruise: 0°	2.6	−16.0	22.2	−12.7	26.7	−12.4
Cruise: 40°	−0.5	−9.6	24.7	−6.8	34.1	−6.3
Descent: 0°	2.3	−22.2	22.1	−24.3	27.2	−24.3
Descent: 40°	1.3	−13.6	27.0	−14.6	40.4	−14.3

4.1. Differences Between Operating Conditions

The analysis revealed distinct sonic boom characteristics for the selected supersonic operating conditions climb, cruise, and descent with both modeling approaches. Each flight condition demonstrated unique behavior in terms of peak pressure and signal duration and the Carlson method showed some capability in capturing these distinctions. The sonic boom carpet width is not captured by the simplified method but showed significant distinctions between the three atmospheric models used for the higher-fidelity simulations as can be seen in Figure 8.

4.1.1. Climb Condition

The climb condition was picked at 15 km of altitude at Mach 1.5 and a flight path angle of 1.15°. The associated angle of attack was 4.5°. This condition consistently showed the highest sonic boom peak pressures and loudness levels on the ground. The larger angle of attack during the climb, combined with lower flight altitudes, resulted in higher lift, which resulted in the highest near-field shock wave amplitudes and the lowest distance to the ground. The simplified method accurately predicted that the climb condition would produce the highest peak amplitudes (see Table 3), although it does not account for the angle of attack. This indicates that the low altitude of 15 km is the principal driver of the increased sonic boom levels on the ground and not so much the higher shock wave amplitudes due to lift.

The study does not take into account acceleration effects, which would supposedly lead to focused booms and higher loudness levels on the ground during climb [55] and higher variability due to atmospheric effects [64]. This indicates, that the climb and acceleration phase from low altitudes and Mach numbers will impose the biggest challenge for future supersonic operational procedures in terms of sonic boom mitigation.

4.1.2. Cruise Condition

The cruise condition was defined as a Mach 2 steady climb cruise with a flight path angle of 0.02° at an altitude of 18.5 km and an angle of attack of 3.5°. The sonic boom simulations resulted in the lowest peak amplitude and shortest signal duration, which can be explained by the long distance to the ground and the high velocity, respectively. The higher Mach number during cruising results in a sharper Mach cone, which leads to a wider lateral spread of the sonic boom carpet (Figure 8). While the Carlson method effectively captured the reduction in sonic boom intensity compared to the climb, it did not predict the signal duration to be the shortest in that operating condition. This might indicate, that the Mach number impact on signal duration is under-predicted in Carlson's formula, or that the opposing influence of altitude is over-predicted in this case.

4.1.3. Descent Condition

The descent condition produced results that fell between those of climb and cruise. This seems reasonable, as the condition has the same Mach number as the climb (Mach 1.5) while being at almost the altitude of the cruise condition (17.5 km). The flight path angle is at −1.17° at an angle of attack of 4.0°. The higher altitude during descent apparently led to a reduction in peak pressures compared to the climb, while the signal duration remained relatively long due to the lower Mach number. The Carlson method captured this reduction in amplitude reasonably well, as illustrated in Table 3.

4.2. Comparison of Modeling Methods

The simplified model effectively distinguishes between the flight phases under consideration (i.e., climb, cruise, and descent) by indicating how changes in Mach number, altitude, and flight path angle influence both the peak amplitude and signal duration of sonic boom N-waves. For example, the method correctly predicted that the climb condition would generate the strongest amplitudes. Studies in the literature compare analytical methods with high-fidelity methods for the early stages of the conceptual design of new

generations of supersonic aircraft. Graziani et al. [18] compared the same aircraft in a validation case study with unrealistic flight conditions. Scarselli in his previous works [21,22] evaluates a sonic boom minimization approach by adopting the Carlson method and compares the results with CFD results [20]. When comparing the simplified predictions to the higher-fidelity predictions in the standard atmosphere, the simplified method over-predicted peak pressure during descent while under-predicting it during climb. For the signal duration, however, a general under-prediction of up to −27% was observed in comparison to the higher-fidelity results (see Table 10). This behavior was already described in earlier comparative studies for a verified clean configuration of the reference aircraft [18]. The signal duration is a parameter, which is sometimes used to compute loudness values from N-waves, which was not conducted in this study.

However, it is clear that the high-fidelity model provides more precision, particularly in non-standard atmospheric conditions, such as those seen in the SBPW3 cases. Neglecting the atmospheric effects significantly reduces the accuracy of sonic boom predictions [65]. Also, in our study the detailed analysis of the geometric extent of the sonic boom carpet and the exact pressure wave-forms at different azimuth angles revealed complexities that the Carlson method could not fully address, such as the influence of wind and individual stratified atmospheric profiles which have been studied before in greater detail [46,66,67]. In these scenarios, the high-fidelity model captured significant variations in boom intensity and the extent of the carpet, which cannot be modeled with the simplified prediction method.

4.3. Implications for Future Supersonic Design and Sonic Boom Modeling

The high-fidelity results for this conventional supersonic aircraft design showed that the shock wave on the ground reached an almost ideal N-wave behavior under all conditions. This means the Carlson method's main assumption of N-wave behavior remains valid for the reference aircraft. However, future low boom aircraft might change the shock wave behavior, such that the assumption of an N-wave on the ground could be rejected.

In summary, the Carlson method remains a useful and effective tool for early assessments of the sonic boom characteristics of conventional supersonic aircraft. It was also proven useful in distinguishing between different flight conditions like climb, cruise, and descent. It captures the broad trends in sonic boom intensity and, to a lesser extent, signal duration across these conditions, providing a valuable initial method for evaluating sonic boom of supersonic aircraft designs. The order of deviation observed when comparing the Carlson predictions with high-fidelity results helps identify where more detailed modeling is warranted, especially in complex atmospheric conditions or for low-boom configurations.

A combination of ray-tracing to predict geometric sonic boom carpet properties under realistic conditions, coupled with a Carlson estimation of the maximum sonic boom peak amplitude, could be an efficient medium-fidelity sonic boom prediction method, as CFD shock wave simulation in the near-field, and non-linear dissipative shock wave propagation in the far-field domain are by far the most complex and computationally intensive procedures of the higher-fidelity approach. Additionally, a simplified method to model wind effects on geometric sonic boom carpet spreading could improve the simplified predictions.

5. Conclusions

The study provided a detailed comparison between the bi-domain high-fidelity non-linear propagation method and the simplified Carlson method for predicting sonic boom characteristics across different supersonic flight conditions (climb, cruise, and descent), which were selected from a realistic operation scenario of a Concorde-like supersonic reference aircraft. The results indicate that the Carlson method is capable of capturing general trends, including variations in peak amplitude and signal duration due to changes in Mach number, altitude, and flight path angle. The influence of realistic weather scenarios with winds is, however, not included in the modeling approach, such that their significant impact on sonic boom carpet width and peak amplitude cannot be represented.

The Carlson method effectively highlights differences between operating conditions, making it a valuable tool during the early stages of conventional supersonic aircraft design. However, the high-fidelity model is essential for capturing the nuanced impacts of atmospheric stratification and wind effects, which are crucial for regulatory compliance and public acceptance of supersonic travel.

Future work should focus on refining the simplified method to account for more atmospheric variables, potentially enhancing its applicability for more realistic flight scenarios. Additionally, incorporating acceleration effects during climb and descent could provide a more comprehensive understanding of the sonic boom characteristics during supersonic operation.

Author Contributions: Conceptualization, J.J., S.G. and F.P.; Formal analysis, J.J., S.G., A.G. and F.P.; Investigation, J.J.; Methodology, J.J., S.G. and F.P.; Project administration, J.J., F.P. and V.G.; Software, J.J., S.G. and A.G.; Supervision, F.P. and V.G.; Visualization, J.J., S.G. and A.G.; Writing original draft, J.J., S.G. and A.G.; Writing review and editing, F.P. and V.G. All authors have read and agreed to the published version of the manuscript.

Funding: This research was funded by the European Union's Horizon 2020 research and innovation program under grant agreement No. 101006856, project MORE&LESS (MDO and Regulations for Low-boom and Environmentally Sustainable Supersonic Aviation).

Institutional Review Board Statement: Not applicable.

Informed Consent Statement: Not applicable.

Data Availability Statement: The original data presented in the study are openly available in ZENODO at https://doi.org/10.5281/zenodo.13972010.

Acknowledgments: The authors would like to thank all the partners of the MORE&LESS project. We thank Nicolle Raspe for creating Figure 3 and re-creating Figure 1 based on the original work by [16].

Conflicts of Interest: The authors declare no conflicts of interest. The results, opinions, conclusions, etc., presented in this work are those of the authors only.

Abbreviations

The following abbreviations are used in this manuscript:

AIAA	American Institute of Aeronautics and Astronautics
CFD	Computational Fluid Dynamics
CS1	Case Study 1
ESATTO	Environmentally Sustainable AircrafT Trajectory and Operations
ICAO	International Civil Aviation Organization
ISA	International Standard Atmosphere
ISBAP	Indoor Sonic Boom Annoyance Predictor
MORE&LESS	MDO and Regulations for Low-boom and Environmentally Sustainable Supersonic aviation
NASA	National Aeronautics and Space Administration
PL	Stevens' Mk VII Perceived Level of Noise
SBPW	Sonic Boom Prediction Workshop
SEL	Sound Exposure Level

References

1. Maglieri, D.J.; Bobbitt, P.J.; Plotkin, K.J.; Shepherd, K.P.; Coen, P.G.; Richwine, D.M. *Sonic Boom: Six Decades of Research*; NASA Langley Research Center: Hampton, VA, USA, 2014.
2. Rötger, T.; Eyers, C.; Fusaro, R. A Review of the Current Regulatory Framework for Supersonic Civil Aircraft: Noise and Emissions Regulations. *Aerospace* **2024**, *11*, 19. [CrossRef]
3. Liebhardt, B.; Gollnick, V.; Luetjens, K. Estimation of the Market Potential for Supersonic Airliners via Analysis of the Global Premium Ticket Market. In Proceedings of the Aviation Technology, Integration, and Operations (ATIO) Conferences, Virginia Beach, VA, USA, 20–22 September 2011. [CrossRef]

4. Alkaya, C.; Alex Sam, A.; Pesyridis, A. Conceptual Advanced Transport Aircraft Design Configuration for Sustained Hypersonic Flight. *Aerospace* **2018**, *5*, 91. [CrossRef]
5. Aronstein, D.C.; Schueler, K.L. Two Supersonic Business Aircraft Conceptual Designs with and without Sonic Boom Constraint. *J. Aircr.* **2005**, *42*, 775–786. [CrossRef]
6. Furukawa, T.; Makino, Y. Conceptual Design and Aerodynamic Optimization of Silent Supersonic Aircraft at JAXA. In Proceedings of the 25th AIAA Applied Aerodynamics Conference. American Institute of Aeronautics and Astronautics (AIAA), Miami, FL, USA, 25–28 June 2007. [CrossRef]
7. Sun, Y.; Smith, H. Review and prospect of supersonic business jet design. *Prog. Aerosp. Sci.* **2017**, *90*, 12–38. [CrossRef]
8. Rathsam, J.; Coen, P.; Loubeau, A.; Ozoroski, L.; Shah, G. Scope and goals of NASA's Quesst Community Test Campaign with the X-59 aircraft. In Proceedings of the 14th ICBEN Congress on Noise as a Public Health Problem, Belgrade, Serbia, 18–22 June 2023.
9. Loubeau, A.; Naka, Y.; Cook, B.G.; Sparrow, V.W.; Morgenstern, J.M. A new evaluation of noise metrics for sonic booms using existing data. *AIP Conf. Proc.* **2015**, *1685*, 090015. [CrossRef]
10. Doebler, W.; Wilson, S.; Loubeau, A.; Sparrow, V. Five-year simulation study of NASA X-59 low-boom carpets across the contiguous United States of America. In Proceedings of the eForum Acusticum 2020, Online, 7–11 December 2020; pp. 1001–1008. [CrossRef]
11. Carr, A.N.; Lonzaga, J.B.; Miller, S.A. Numerical prediction of loudness metrics for N-waves and shaped sonic booms in kinematic turbulence. *J. Acoust. Soc. Am.* **2022**, *151*, 3580–3593. [CrossRef]
12. Doebler, W.J.; Sparrow, V.W. Stability of sonic boom metrics regarding signature distortions from atmospheric turbulence. *J. Acoust. Soc. Am.* **2017**, *141*, EL592–EL597. [CrossRef]
13. Graziani, S.; Petrosino, F.; Jäschke, J.; Glorioso, A.; Fusaro, R.; Viola, N. Evaluation of Sonic Boom Shock Wave Generation with CFD Methods. *Aerospace* **2024**, *11*, 484. [CrossRef]
14. Cleveland, R.O.; Hamilton, M.F.; Blackstock, D.T. Time–domain modeling of finite–amplitude sound in relaxing fluids. *J. Acoust. Soc. Am.* **1996**, *98*, 2865. [CrossRef]
15. Rallabhandi, S.K. Advanced Sonic Boom Prediction Using the Augmented Burgers Equation. *J. Aircr.* **2011**, *48*, 1245–1253. [CrossRef]
16. Park, M.; Morgenstern, J. Summary and Statistical Analysis of the First AIAA Sonic Boom Prediction Workshop. In Proceedings of the 32nd AIAA Applied Aerodynamics Conference, Atlanta, GA, USA, 16–20 June 2014; Volume 53. [CrossRef]
17. Carlson, H.W. *Simplified Sonic-Boom Prediction*; Technical report; NASA Langley Research Center: Hampton, VA, USA, 1978.
18. Graziani, S.; Viola, N.; Petrosino, F.; Jäschke, J. Comparison between simplified approach and CFD & Propagation tool for sonic boom estimation. In Proceedings of the AIAA AVIATION 2023 Forum, San Diego, CA, USA, 12–16 June 2023; American Institute of Aeronautics and Astronautics: Reston, VA, USA, 2023. [CrossRef]
19. Bonavolontà, G.; Lawson, C.; Riaz, A. Review of sonic boom prediction and reduction methods for next generation of supersonic aircraft. *Aerospace* **2023**, *10*, 917. [CrossRef]
20. Scarselli, G.; Marulo, F.; Averardo, M.; Cafiero, A.; Selmin, V. Numerical comparison between a simplified method and a full CFD approach for sonic boom evaluation on supersonic innovative configurations. In Proceedings of the 13th AIAA/CEAS Aeroacoustics Conference (28th AIAA Aeroacoustics Conference), Rome, Italy, 21–23 May 2007. [CrossRef]
21. Scarselli, G.; Castorini, E. Preliminary Optimization of the Sonic Boom Properties for Civil Supersonic Aircraft. *J. Aircr.* **2013**, *50*, 1295–1299. [CrossRef]
22. Scarselli, G.; Marulo, F. Sonic Boom Minimization Through a Simplified Approach for the Preliminary Design of Civil Supersonic Aircraft. In Proceedings of the 16th AIAA/CEAS Aeroacoustics Conference, Stockholm, Sweden, 7–9 June 2010; p. 4006.
23. Horizon2020. MDO and Regulations for Low-Boom and Environmentally Sustainable Supersonic Aviation. 2021. Available online: https://cordis.europa.eu/project/id/101006856 (accessed on 16 October 2024). [CrossRef]
24. Park, M.A.; Aftosmis, M.J.; Campbell, R.L.; Carter, M.B.; Cliff, S.E.; Bangert, L.S. Summary of the 2008 NASA Fundamental Aeronautics Program Sonic Boom Prediction Workshop. *J. Aircr.* **2014**, *51*, 987–1001. [CrossRef]
25. Park, M.A.; Nemec, M. Nearfield Summary and Statistical Analysis of the Second AIAA Sonic Boom Prediction Workshop. *J. Aircr.* **2019**, *56*, 851–875. [CrossRef]
26. Park, M.A.; Carter, M.B. Nearfield Summary and Analysis of the Third AIAA Sonic Boom Prediction Workshop C608 Low Boom Demonstrator. In Proceedings of the AIAA Scitech 2021 Forum, Online, 11–15 January 2021. [CrossRef]
27. Carter, M.B.; Park, M.A. Near Field Summary and Analysis of the Third AIAA Sonic Boom Prediction Workshop Shock-Plume Interaction Case. In Proceedings of the AIAA Scitech 2021 Forum, Virtual Event, 11–15 and 19–21 January 2021. [CrossRef]
28. Economon, T.D.; Palacios, F.; Copeland, S.R.; Lukaczyk, T.W.; Alonso, J.J. SU2: An Open-Source Suite for Multiphysics Simulation and Design. *AIAA J.* **2016**, *54*, 828–846. [CrossRef]
29. Shima, E.; Kitamura, K.; Haga, T. Green–gauss/weighted-least-squares hybrid gradient reconstruction for arbitrary polyhedra unstructured grids. *AIAA J.* **2013**, *51*, 2740–2747. [CrossRef]
30. Glorioso, A.; Petrosino, F.; Aprovitola, A.; Barbarino, M.; Pezzella, G. Sonic Boom generation using open source CFD approach. In Proceedings of the AIAA AVIATION 2023 Forum, San Diego, CA, USA, 12–16 June 2023. [CrossRef]
31. Potapkin, A.; Korotaeva, T.; Moskvichev, D.; Shashkin, A.; Maslov, A.; Silkey, J.; Roos, F. An Advanced Approach for Far-Field Sonic Boom Prediction. In Proceedings of the 47th AIAA Aerospace Sciences Meeting including The New Horizons Forum and Aerospace Exposition, Orlando, FL, USA, 5–8 January 2009. [CrossRef]

32. Siclari, M.J.; Darden, C.M. Euler code prediction of near-field to midfield sonic boom pressure signatures. *J. Aircr.* **1993**, *30*, 911–917. [CrossRef]
33. Ozcer, I. Sonic Boom Prediction Using Euler/Full Potential Methodology. In Proceedings of the 45th AIAA Aerospace Sciences Meeting and Exhibit, Reno, NV, USA, 8–11 January 2007. [CrossRef]
34. Roe, P.L. Characteristic-Based Schemes for the Euler Equations. *Annu. Rev. Fluid Mech.* **1986**, *18*, 337–365. [CrossRef]
35. Yamashita, R.; Suzuki, K. Full-Field Sonic Boom Simulation in Real Atmosphere. In Proceedings of the 32nd AIAA Applied Aerodynamics Conference, Atlanta, GA, USA, 16–20 June 2014. [CrossRef]
36. Dagrau, F.; Loseille, A.; Din, I.S.E. Computational and Experimental Assessment of Models for the First AIAA Sonic Boom Prediction Workshop Using Adaptive High Fidelity CFD methods. In Proceedings of the 32nd AIAA Applied Aerodynamics Conference, Atlanta, GA, USA, 16–20 June 2014. [CrossRef]
37. Glorioso, A.; Petrosino, F.; Barbarino, M.; Pezzella, G.; Viviani, A. Improvement on open source CFD methodology to evaluate near-field Sonic Boom. In Proceedings of the 30th AIAA/CEAS Aeroacoustics Conference (2024), Rome, Italy, 4–7 June 2024; p. 3185.
38. Toro, E.F. The HLLC Riemann solver. *Shock Waves* **2019**, *29*, 1065–1082. [CrossRef]
39. Anderson, G.R.; Aftosmis, M.J.; Nemec, M. Cart3D Simulations for the Second AIAA Sonic Boom Prediction Workshop. *J. Aircr.* **2019**, *56*, 896–911. [CrossRef]
40. Onyeonwu, R.O. *The Effects of Wind and Temperature Gradients on Sonic Boom Corridors*; UTIAS Technology Note; No. 168, AFOSR-TR-71-3087; University of Toronto Institute for Aerospace Studies: Toronto, ON, Canada, 1971.
41. Yamamoto, M.; Hashimoto, A.; Aoyama, T.; Sakai, T. A unified approach to an augmented Burgers equation for the propagation of sonic booms. *J. Acoust. Soc. Am.* **2015**, *137*, 1857–1866. [CrossRef] [PubMed]
42. Whitham, G.B. The flow pattern of a supersonic projectile. *Commun. Pure Appl. Math.* **1952**, *5*, 301–348. [CrossRef]
43. Kirz, J. *Numerical Near-Field Simulations of Low Boom Aircraft Concepts*; German Aerospace Society: Bonn, Germany, 2020. [CrossRef]
44. Loubeau, A.; Wilson, S.R.; Rathsam, J. Updated evaluation of sonic boom noise metrics. In Proceedings of the 176th Meeting of the Acoustical Society of America, Victoria, BC, Canada, 8 November 2018; NF1676L-30234.
45. Loubeau, A.; Page, J. Human perception of sonic booms from supersonic aircraft. *Acoust. Today* **2018**, *14*, 23–30.
46. Doebler, W.J. Estimated ambient sonic boom metric levels and X-59 signal-to-noise ratios across the USA. In Proceedings of the Meetings on Acoustics, Online, 5–9 October 2020; Volume 42, Number 1.
47. Stevens, S.S. Perceived Level of Noise by Mark VII and Decibels (E). *J. Acoust. Soc. Am.* **1972**, *51*, 575–601. [CrossRef]
48. Bolander, C.R.; Hunsaker, D.F.; Shen, H.; Carpenter, F.L. Procedure for the Calculation of the Perceived Loudness of Sonic Booms. In Proceedings of the AIAA Aviation 2019 Forum, Dallas, TX, USA, 17–21 June 2019; American Institute of Aeronautics and Astronautics: Reston, VA, USA, 2019. [CrossRef]
49. Acoustics—Description, Measurement and Assessment of Environmental Noise—Part 1: Basic Quantities and Assessment Procedures. 2016. Available online: https://www.iso.org/standard/59765.html (accessed on 16 October 2024).
50. Loubeau, A. Evaluation of the effect of aircraft size on indoor annoyance caused by sonic booms. *J. Acoust. Soc. Am.* **2014**, *136*, 2223–2224. [CrossRef]
51. Roncioni, P.; Marini, M.; Gori, O.; Fusaro, R.; Viola, N. Aerodatabase Development and Integration and Mission Analysis of a Mach 2 Supersonic Civil Aircraft. *Aerospace* **2024**, *11*, 111. [CrossRef]
52. Ferretto, D.; Fusaro, R.; Viola, N. A conceptual design tool to support high-speed vehicle design. In Proceedings of the AIAA AVIATION 2020 FORUM, Virtual Event, 15–19 June 2020. [CrossRef]
53. Van den Borre, K.; Ispir, A.C.; Cakir, B.O.; Saracoglu, B.H. Reduced Order Computational Methods for the Development of Propulsive Technologies for Supersonic Aviation to Achieve Climate Neutrality. In *Advanced Computational Methods and Design for Greener Aviation*; Springer: Berlin/Heidelberg, Germany, 2024; pp. 95–107.
54. ASTOS Solutions GmbH. *ASTOS*, Version 2023; Computer Software; Astos Solutions GmbH: Stuttgart, Germany, 2023.
55. Maglieri, D.J.; Bobbitt, P.J.; Massey, S.J.; Plotkin, K.J.; Kandil, O.A.; Zheng, X. *Focused and Steady-State Characteristics of Shaped Sonic Boom Signatures: Prediction and Analysis*; Technical report; NASA Langley Research Center: Hampton, VA, USA, 2011.
56. *Manual of the ICAO Standard Atmosphere: Extended to 80 kilometres (262 500 feet) = Manuel de l'Atmosphère Type OACI: élargie Jusqu'à 80 kilomètres (262,500 pieds) = Manual de la átmosfera tipo de la OACI: Ampliada hasta 80 kilómetros (262,500 pies)*; International Civil Aviation Organization: Montréal, QC, Canada, 1993.
57. Accredited Standards Committee S1, Acoustics; American National Standards Institute; Acoustical Society of America Standards Secretariat. *Method for Calculation of the Absorption of Sound by the Atmosphere*; rev ed.; Standards Secretariat, Acoustical Society of America: New York, NY, USA, 1995.
58. Rallabhandi, S.K.; Loubeau, A. Summary of Propagation Cases of the Third AIAA Sonic Boom Prediction Workshop. *J. Aircr.* **2021**, *59*, 1–17. [CrossRef]
59. NASA Langley Research Center. Sonic Boom Propagation Webpage for SBPW3 Project. Available online: https://lbpw-ftp.larc.nasa.gov/sbpw3/propagation/case1/ (accessed on 25 September 2024).
60. NASA Langley Research Center. Sonic Boom Propagation Webpage for SBPW3 Project. Available online: https://lbpw-ftp.larc.nasa.gov/sbpw3/propagation/case2/ (accessed on 25 September 2024).

61. Emmanuelli, A.; Dragna, D.; Ollivier, S.; Blanc-Benon, P. Sonic boom propagation over real topography. *J. Acoust. Soc. Am.* **2023**, *154*, 16–27. [CrossRef] [PubMed]
62. Dragna, D.; Emmanuelli, A.; Ollivier, S.; Blanc-Benon, P. Sonic boom reflection over urban areas. *J. Acoust. Soc. Am.* **2022**, *152*, 3323–3339. [CrossRef]
63. Leconte, R.; Chassaing, J.C.; Coulouvrat, F.; Marchiano, R. Propagation of classical and low booms through kinematic turbulence with uncertain parameters. *J. Acoust. Soc. Am.* **2022**, *151*, 4207–4227. [CrossRef]
64. Blumrich, R.; Coulouvrat, F.; Heimann, D. Variability of focused sonic booms from accelerating supersonic aircraft in consideration of meteorological effects. *J. Acoust. Soc. Am.* **2005**, *118*, 696–706. [CrossRef]
65. Blumrich, R.; Coulouvrat, F.; Heimann, D. Meteorologically induced variability of sonic-boom characteristics of supersonic aircraft in cruising flight. *J. Acoust. Soc. Am.* **2005**, *118*, 707–722. [CrossRef]
66. Reddy, S.R.; Chitale, J.; Dulikravich, G.S. Effects of Atmospheric Uncertainties on Sonic Boom Perceived Level. *J. Fluids Eng.* **2021**, *143*, 041504. [CrossRef]
67. Iura, R.; Ukai, T.; Yamashita, H.; Kern, B.; Misaka, T.; Obayashi, S. Impact of atmospheric variations on sonic boom loudness over 10 years of simulated flights. *J. Acoust. Soc. Am.* **2024**, *156*, 1529–1542. [CrossRef]